

Highest methane concentrations in an Arctic River linked to local terrestrial inputs.

Karel Castro-Morales^{1*}, Anna Canning², Sophie Arzberger¹, Will A. Overholt¹, Kirsten Küsel^{1,3}, Olaf Kolle⁴, Mathias Göckede⁴, Nikita Zimov⁵, and Arne Körtzinger^{2,6}

¹ Friedrich-Schiller University Jena, Institute of Biodiversity, Jena, Germany.

² GEOMAR Helmholtz Centre for Ocean Research Kiel, Kiel, Germany.

³ German Centre for Integrative Biodiversity Research (iDiv) Halle-Jena-Leipzig, Germany

⁴ Max Planck Institute for Biogeochemistry, Jena, Germany

⁵ Pleistocene Park, Northeast Science Station, Chersky, Russia.

⁶ Christian Albrecht University Kiel, Kiel, Germany

*Correspondence: Karel Castro-Morales (karel.castro.morales@uni-jena.de)

Abstract.

Large amounts of methane (CH₄) could be released as a result of the gradual or abrupt thawing of Arctic permafrost due to global warming. Once available, this potent greenhouse gas is emitted into the atmosphere, or transported laterally into aquatic ecosystems via hydrologic connectivity at surface or groundwaters. While high northern latitudes contribute up to 5 % of total global CH₄ emissions, the specific contribution of Arctic rivers and streams is largely unknown. We analyzed high-resolution continuous CH₄ concentrations measured between 15 and 17 June 2019 (late freshet) in a ~120 km transect of the Kolyma River in Northeast Siberia. The average partial pressure of CH₄ ($p\text{CH}_4$) in tributaries (66.8 – 206.8 μatm) was 2-7 times higher than in the main river channel (28.3 μatm). In the main channel, CH₄ was up to 1600 % supersaturated with respect to atmospheric equilibrium. Key sites along the riverbank and at tributary confluences accounted for 10 % of the navigated transect, and had the highest $p\text{CH}_4$ (41±7 μatm) and CH₄ emissions (0.03±0.004 mmol m⁻² d⁻¹) compared to other sites in the main channel, contributing between 14 to 17 % of the total CH₄ flux in the transect. These key sites were characterized by warm waters ($T>14.5$ °C) and low specific conductivities ($\kappa<88$ $\mu\text{S cm}^{-1}$). The distribution of CH₄ in the river could be linked statistically to T and κ of the water, and to their proximity to the shore z , and these parameters served as predictors of CH₄ concentrations in unsampled river areas. The abundance of CH₄-consuming bacteria and CH₄-producing archaea in the river was similar to those previously detected in nearby soils, and was also strongly correlated to T and κ . These findings imply that the source of riverine CH₄ is closely related with sites near land. The average total CH₄ flux density in the river section was 0.02±0.006 mmol m⁻² d⁻¹, equivalent to an annual CH₄ flux of 1.24×10⁷ g CH₄ yr⁻¹ emitted during a 146-days open water season. Our study highlights the importance of high-resolution continuous CH₄ measurements in Arctic Rivers for identifying spatial and temporal variations, as well as providing a glimpse of the magnitude of riverine CH₄ emissions in the Arctic and their potential relevance to regional CH₄ budgets.

1 Introduction

Methane (CH₄) is a powerful greenhouse gas that absorbs the Earth's infrared radiation more efficiently than CO₂, with a global warming potential 28 times that of CO₂ over a time

horizon of 100 years (Saunois et al., 2020). To date, CH₄ has accounted for 16 to 25 % of the

current atmospheric warming (Etminan et al., 2016; IPCC, 2014; Rosentreter et al., 2021).

Globally, aquatic ecosystems contribute about half (53 %) of the total CH₄ emissions, both from anthropogenic and natural origin (Rosentreter et al., 2021). The total bottom-up (i.e.,

from process-based models and inventories) updated global CH₄ emissions from rivers and streams have a mean of 30.5 ± 17.1 Tg CH₄ yr⁻¹ (Rosentreter et al., 2021), and account for ~17

% of the average inland water CH₄ fluxes (Saunois et al., 2020). Especially on regional scales, CH₄ emissions from rivers and streams have large impacts on the estimation of local

atmospheric emissions (Karlsson et al., 2021). The contribution of CH₄ emissions in high northern latitudes (60 – 90° N) to total global CH₄ emissions ranges between 4 to 5 %, but

there are significant uncertainties, particularly regarding the contributions from terrestrial

permafrost and non-wetland inland waters, i.e., rivers, streams, and lakes (Saunois et al.,

2020). The concentration of CH₄ in rivers and streams is generally above saturation with

respect to the present atmospheric CH₄ concentration, emitting annually the equivalent to ~15 % of the total emissions from wetlands or 40 % of the annual CH₄ emissions from lakes

(Stanley et al., 2016).

The Arctic Ocean is one of the most river-influenced and land-locked of all the world oceans (Charkin et al., 2017; Shakirov et al., 2020), receiving annually about 10 % of the global

runoff (Lammers et al., 2001), through the input from the main six Arctic rivers: Yenisey,

Lena, Ob, Mackenzie, Yukon, and Kolyma. These rivers connect the ocean with the land, by mediating the transport of CH₄ stored in terrestrial surface waters or groundwaters, or through

soil-water interactions in thawed water tracks (Connolly et al., 2020; Dabrowski et al., 2020;

Harms et al., 2020; Saunois et al., 2020). Thus, the riverine transport of soil-derived CH₄ from permafrost may influence the CH₄ concentrations in the Arctic shelf system.

The atmospheric emissions of CH₄ from Arctic inland freshwaters and permafrost have the potential to increase with climate change (Dean et al., 2018). As permafrost thaws, more soil

organic carbon is available for the anaerobic degradation of organic matter under warmer

conditions, resulting in additional CH₄ formation of which will add to the positive feedback to climate change (Schuur et al., 2015). Trapped or newly formed CH₄ can be emitted directly to

the atmosphere after the abrupt or gradual permafrost thaw (Olefeldt et al., 2013; Saunois et

al., 2020; Turetsky et al., 2020), or be laterally transported into neighboring inland waters via

75 surface hydraulic connectivity or underground drainage (e.g., Dabrowski et al., 2020). Current and projected changes in the Arctic land surface hydrology, vegetation, landscape, and temperature due to permafrost thaw, will modulate CH₄ concentrations in Arctic fluvial ecosystems (Harms et al., 2020; Olid et al., 2021).

The magnitude of the fluvial CH₄ emissions is subject to strong local environmental controls, 80 because CH₄ has low solubility in water (Campeau and del Giorgio, 2014; Stanley et al., 2016). At the same time, the abundance and phylogenetic identity of microorganisms in the river water that can be associated to the formation or consumption of CH₄, can serve as indicators of the source and fate of CH₄ transported from land. Aquatic CH₄ is subject to microbial oxidation and photochemical decomposition (Dean et al., 2018; Stanley et al., 85 2016). Little is known about the magnitude of CH₄ concentrations and emissions from flowing Arctic inland waters, as well as how they vary over time and space. Point CH₄ measurements in some Arctic rivers and streams have demonstrated supersaturation relative to the atmosphere (e.g., Kling et al., 1992; Mann et al., 2022; Striegl et al., 2012; Vorobyev et al., 2021; Zolkos et al., 2019). However, highly resolved aquatic CH₄ measurements are 90 lacking in large portions of Arctic rivers and streams, and these are needed to better quantify the atmospheric gas fluxes and understand the temporal variations and the environmental indicators. High-resolution measurements of the partial pressure of CH₄ ($p\text{CH}_4$) were measured in a site in Ambolikha River, a tributary of Kolyma River in northeast Siberia, evidencing aquatic CH₄ supersaturations up of the order of 200 times higher than values at 95 equilibrium with the atmosphere. These measurements allowed identifying temporal variations mostly driven by hydrological changes and air-water exchange, with a consistent decrease of $p\text{CH}_4$ by 78 % from the measured concentrations during late freshet to summer (Castro-Morales et al., 2022).

Here, we present the first high spatial resolution measurements of $p\text{CH}_4$, and other 100 complementary water properties, in a large section of the Kolyma River during the late freshet (June) in 2019. Additionally, we followed the riverine microbial community structure using a 16S-amplicon approach along the same 120 km long transect, to provide a potential record of water input sources. The objectives of this study are: 1) to analyze potential environmental indicators that can be statistically associated with the spatial variations of the $p\text{CH}_4$ along the 105 sampled river section, 2) to estimate the flux of CH₄ across the atmosphere-river interface, and 3) to investigate a potential link between overall microbial community structure and more specifically the distributions of CH₄ oxidizers and CH₄ producers with the measured $p\text{CH}_4$ during the sampling period.

2 Methods

2.1 Study site and fieldwork description

The Kolyma River is the sixth largest river in the Arctic, with a watershed area of 653,000 km² (Holmes et al., 2012), that is completely underlain by continuous permafrost (Mann et al., 2012). Our area of study was a ~120 km section in the Kolyma River, bounded by the city of Chersky (68° 45' 5.1" N, 161° 18' 16.6" E) to the east and at the location known as Duvannyi Yar (68° 38' 12.8" N, 159° 5' 25.4" E) to the west (Fig. 1). Several floodplains are located next to the banks of this section of the Kolyma River. These floodplains connect the river to the land during the snow melt period (May and June) when they become inundated. We twice navigated the Kolyma River section onboard a small vessel (average navigation speed of 2.0 ± 0.4 m s⁻¹), where we installed our instruments for measurements of continuous water properties and the partial pressure of CH₄ ($p\text{CH}_4$) (Sect. 2.2.). The first transect was navigated in the upstream direction (UP) from Chersky to Duvannyi Yar (Fig. 1) between 15 June 2019 (12:48 h; local Chersky time) and 16 June 2019 (16:59 h) (with an overnight break halfway), covering a length of 127.7 km. The second transect was navigated in the downstream direction (DOWN) from Duvannyi Yar to Chersky, and took place between 16 June 2019 (17:00 h) and 17 June 2019 (13:27 h), covering a length of 115.4 km. In 2019, the ice break-up in Kolyma River at Chersky started on 1 June, and our sampling took place during the late freshet. Thus, during the sampling campaign the transect navigated was completely ice-free and in the decreasing phase of the freshet peak discharge as shown by the daily records from the gauge station Kolymsk-1 (68° 43' 48" N, 158° 43' 12" E) in the Kolyma River (Fig. S1). During the sampling days, the average width of the Kolyma channel was about 2 km. With help of the Arctic DEM Explorer (Environmental Systems Research Institute, Polar Geospatial Center; <https://livingatlas2.arcgis.com/arcticdemexplorer/>), we estimated a total area of the sampled Kolyma River section of about 221 km². Continuous water properties were measured along both transects (Sect. 2.2). The vessel primarily navigated at the center of the Kolyma River main channel during the sampling, particularly in the DOWN transect. We purposely navigated in the proximity of the confluences of tributaries and in banks adjacent to floodplains during the UP transect to capture the water properties in regions with visually evident, large lateral contributions from land (i.e., runoff from land as evidenced by more turbid and/or differently colored water). To facilitate the analysis of the high-resolution data and analyze the specific contribution of banks and confluences with tributaries to the measured water properties and $p\text{CH}_4$, we defined five key sites (i.e., S1 to S5) that are associated with sampling points along the UP transect.

From east to west the location of the “key sites” is: S1, bank of floodplain 1 at Ambolikha river in station PP07; S2, the confluence of tributaries Maly Anyuy and Bolshoy Anyuy (M&B Anyuy) in station PP11; S3, bank of floodplain 2 (only in DOWN transect) in station PP20; S4, bank of floodplain 3 (only in UP transect) in station PP23; and, S5, bank at Duvannyi Yar in station PP25 (Fig. 1). The separation between “key sites” and the “other sites” of the data was done on the basis of the measured $p\text{CH}_4$, T and κ in the UP and DOWN transects, and also analyzed independently for each transect.

The UP and DOWN transects were not navigated exactly at the same locations and the geographical overlap took place only in a few areas (Fig. 1). Therefore, we compare the results between these transects in the context of the temporal variability of the measured parameters, while the spatial variation is done between the key and other sites of the areas for each transect.

2.2 Collection of discrete river water samples and analysis

During the UP transect, we collected discrete water samples at 21 sampling stations (PP05-PP25) distributed along the track (see Fig. 1 for location and Table S1 for sampling times and average water properties measured at each station), for the analysis of total organic carbon (TOC) and the composition of microbial communities (Sect. 2.3.). For this, a 1.5 L Niskin bottle was lowered to 1 m depth and water samples were drawn from the sampler onboard through silicone tubing.

2.2.1 Analysis of Total Organic Carbon (TOC) in river water samples

For the quantification of TOC, a volume of 250 mL of water was transferred from the Niskin bottle into an acid-washed amber glass flask. The samples were stored at 4 °C until pre-treatment at the laboratory of the Northeast Science Station in Chersky after the sampling campaign. The samples were brought to room temperature and manually homogenized. Two aliquots of 10 mL were transferred to acid-washed glass vials and acidified to pH 2.0 with 37 % HCl. The samples were kept cold during storage and transport to Germany for the determination of TOC via high-temperature catalytic combustion (Analytik Jena), with each sample measured from three to five times as analytical replicates. Due to the loss of samples, we report results of TOC in water samples from 7 out 21 stations (33 %).

2.2.2 Analysis of microbial communities in river water samples

We determined the distribution and total community composition of microbial communities, including CH_4 -producing archaea (methanogens) and CH_4 -oxidizing bacteria (methanotrophs and methylotrophs) in the river water samples. Methanotrophs utilize CH_4 as carbon source, whereas methylotrophs are more versatile and can also use other C1 compounds as carbon

source. In addition, the abundance of bacteria and archaea was determined along the transects. For this, a volume of 500 mL of the surface river water from the Niskin bottle was transferred into a 500 mL glass flask (DURAN® Borosilicate glass, SCHOTT). Using a hand pump and
180 filtration system, this sample was immediately filtered on board through a 0.2 µm filter (Supor®). The 500 mL were divided into three aliquots and filtered independently for analytical replication. The filters were stored inside 2 mL sterile Biozym tubes and submerged in DNA/RNA shield solution (Zymo Research). The tubes with the filters remained at room temperature for their subsequent transport and analysis in Germany for DNA isolation,
185 amplicon sequencing, and 16S rRNA gene quantification following protocols specified in the supplementing text S.1.2. and S.1.3.

2.3 Instrumental setup

Two instruments were installed onboard the vessel for continuous measurements of water properties: (1) an EXO2 multiparameter sonde with seven sensors for simultaneous optical
190 and non-optical water measurements (Sect. 2.3.1), and (2) a Flow-Through (FT) system for continuous measurements of the partial pressure of CH₄ ($p\text{CH}_4$) (Sect. 2.3.2). The instruments were continuously fed with water pumped from the port side of the vessel from a nominal depth of 1 m below the water surface, hereinafter referred to as “surface water”. The surface water was delivered through a PVC tubing of 2.5 m length and split into two outlets: 1) to
195 feed the FT system at an approximate flow rate of 0.14 L s⁻¹, and 2) to a 20-L FT box located onboard where the EXO2 probe was immersed for the continuous surface water measurements.

2.3.1 EXO2 Sonde

The EXO2 multiparameter sonde (YSI Inc., Xylem Inc., Yellow Springs, OH, USA) was used
200 to measure optically the turbidity (in formazin nephelometric units, FNU), dissolved O₂ (DO, µmol L⁻¹), and fluorescent dissolved organic matter ($f\text{DOM}$; Quinine Sulfate Units, QSU) of the incoming surface river water. It also measured temperature-corrected conductivity (specific conductivity, κ in µS cm⁻¹) with conductivity electrodes, water temperature (T , °C) with a thermistor, and pH with a glass electrode. The sonde had an internal battery and was
205 mounted inside a metal frame (to provide protection and stability) submerged inside the 20 L FT box that received the incoming water pumped from the surface. The bucket was kept covered with a lid to avoid heating of the water and light exposure of the sensors. Considering the same water flow rate at the FT box as in the FT system, the water retention time in the FT box was on average 2.3 min, which allowed a sufficient time for the sensors in the probe to
210 stabilize for a reliable measurement.

The sonde was equipped with a wiper brush that was used routinely to clean the window of the sensors to avoid interferences due to fouling caused by the accumulation of deposits. The wiping periods were registered and removed from the data set. We obtained one measurement every 5 sec and the data was monitored and stored in a computer onboard.

As a result of the travel distance of the pumped water through the pipe (see Sect. S.1.1 for details), the water within the 20 L bucket on board was on average 0.6 °C warmer and with 1.2 mg L⁻¹ higher DO content than the in-situ water at 1 m depth. Thus, the EXO2 sonde *T* and DO measurements were corrected by these mean values. All the sensors of the sonde were factory-calibrated previous to the measurements. Two-point calibrations were performed on-site to the DO and pH sensors and no analytical drift was observed before and after the measurements that would have required correction. The measured *f*DOM was temperature corrected to a reference of 25 °C (Downing et al., 2012; Watras et al., 2011), and further corrections due to the turbidity influence in the sensor response to light attenuation were done after Snyder et al. (2018).

2.3.2 Flow-through (FT) system

The FT system is a portable and versatile flow-through sensor set-up for continuous direct measurements of *p*CH₄ from surface water. We used a CONTROS HydroC[®] CH₄ FT sensor based on tunable diode laser absorption spectroscopy (TDLAS) (-4H-JENA engineering GmbH, Jena, Germany). This sensor has a working accuracy of ±2 µatm or 3 % of the reading (Canning et al., 2021a) according to the manufacturer standard specifications. A SBE45 thermosalinograph sensor (Sea-Bird Electronics, Bellevue, USA) was used to measure the temperature (*T*_{FT}, °C) and conductivity of the incoming water. The HydroC[®] CH₄ FT sensor was factory-calibrated before and after the measurement campaign. The calibration and validation of the data were done following Canning et al. (2021a). Drift and response time corrections were not applied because we assume sufficient exposure of the water to the sensor at the low sailing speeds. Because the relatively long response time of the CH₄ sensor (of the order of 20 min), the obtained data are significantly smoothed and therefore, the captured gradients and extreme values might not be precisely geographically located. However, the advantage of the high-spatial-resolution data allowed for a surface coverage that help identify high CH₄-concentration areas. For more in-depth corrections see Canning et al. (2021a).

Besides the slow navigation speed, the average time spent at each sampling station was 7±13 min (minimum of 2 min and maximum of 8 min), which allowed for further equilibration times of the surface water at the sensors of the instruments, particularly at sites with high

245 CH₄ concentration.

We obtained one measurement every 5 sec and the data were monitored and stored on a computer onboard. The EXO2 sonde and FT system data were averaged to 1 min values. During the measurements, we also navigated inside smaller tributaries, one located at halfway along the transect length (named here as Leonid's stream), and another at the end
250 of the DOWN transect, located along the Ambolikha River. Because the water properties measured in these streams are very contrasting to the properties in the main stem, we removed these sections from the full data, but still present the average values measured along those transects.

2.4 CH₄ flux calculation

255 To obtain the gas exchange across the water-air interface (i.e., flux density) it is necessary to calculate the gas transfer velocities k . Here we followed two methods to obtain k : 1) using a hydraulic model as a function of water velocity and discharge, and the river configuration (Raymond et al., 2012), and 2) using a parameterization as a function of wind speed (Wanninkhof, 2014). This was done in order to cover a range of values given the large
260 uncertainties of k in rivers.

The hydraulic model that we used to calculate k , is a function of stream velocity (V , m s⁻¹), river slope (S , unitless), water discharge (Q , m³ s⁻¹), and water depth (D , m) (empirical Eq. 7 in Raymond et al., 2012):

$$k_{R12} = 4725 \times (VS)^{0.86} \times Q^{-0.14} \times D^{0.66} \quad (1)$$

265 The average stream velocity for the transect ($V=1.27\pm0.1$ m s⁻¹) was calculated from the mean daily water discharge from 15 to 17 June 2019 as reported at the gauge station Kolymsk-1 ($Q=13267\pm950$ m³ s⁻¹) divided by the mean cross-sectional area in the channel ($A=10400\pm9721$ m²). A was calculated from the average river depth ($D=5.2\pm4.9$ m) times the river width (W fixed at 2000 m) at the sampling times. The slope S for the Kolyma River
270 along the 120 km channel was 0.003 % considering the mean elevation of 4 m, obtained from the slope map in the Arctic DEM Explorer (Environmental Systems Research Institute, Polar Geospatial Center; <https://livingatlas2.arcgis.com/arcticdemexplorer/>). An uncertainty of up to 7.8 % is obtained in this calculation mostly due to the use of an average river depth for the calculation of the cross-sectional area and the stream velocity. The section of the Kolyma
275 River can be in places as shallow as 1.7 m and as deep as 21.6 m, leading to faster water flows as the water column is shallow. However, larger uncertainties are expected due to the variation in Q along the stream, since the values used here are daily averages measured at once single site at the Kolymsk-1 gauge station.

The empirical wind speed parameterization is used to also calculate k , followed by

280 Wanninkhof (2014):

$$k_{W14} = 0.251 \times (u_{10})^2 \quad (2)$$

Where u_{10} (m s^{-1}) is the wind speed normalized to 10 m above the water surface, following Amorocho and Devries (1980), calculated from the wind velocities measured at a height of 6 m above ground at a nearby eddy tower during the sampling period (Castro-Morales et al., 285 2022).

The k_{R12} from the hydraulic model and k_{W14} from the wind parameterization were standardized to a constant temperature using the Schmidt number (Sc) for CO_2 and freshwater at 20 °C, i.e., $Sc_{\text{CO}_2}=600$ (Wanninkhof, 1992), and the Sc of CH_4 (Sc_{CH_4}) (Wanninkhof, 2014) following:

$$290 \quad k_* = k_- \times \left(\frac{Sc_{\text{CH}_4}}{Sc_{\text{CO}_2}} \right)^{-0.5} \quad (3)$$

The water-to-air flux density of CH_4 (F , $\text{amount area}^{-1} \text{ time}^{-1}$) was obtained with the following function: $F_* = k_* \cdot (C_w - C_{eq})$, where k_* is the gas transfer velocity (length time^{-1}) of CH_4 at the in-situ T (Eq. 3) for R12 or W14 (Eq. 1 and 2). The water-side equilibrium concentration of CH_4 (C_{eq} , $\mu\text{mol L}^{-1}$) is subtracted from the measured bulk CH_4 concentration 295 in the water (C_w , $\mu\text{mol L}^{-1}$). C_w was calculated from the Bunsen solubility coefficient (β , $\text{mol L}^{-1} \text{ atm}^{-1}$) that is calculated as a function of temperature Weiss (1970), while C_{eq} was calculated following Wiesenburg and Guinasso (1979). The atmospheric $p\text{CH}_4$ (atm) was calculated following:

$$p = x(P - p_{\text{H}_2\text{O}}) \quad (4)$$

300 where x is the dry air mole fraction of CH_4 . P is the barometric pressure and $p_{\text{H}_2\text{O}}$ is the saturation water vapor pressure at in-situ water temperature (both in atm). We used the global mean dry air mole fraction of 1858.8 ppb for CH_4 during June 2019 according to the Global Monitoring Laboratory, NOAA (Dlugokencky and Tans, 2019), and a standard barometric pressure of 1 atm.

305 **2.5 Data analysis**

2.5.1 Correlation between water $p\text{CH}_4$ and water parameters

To simplify the analysis for finding the relationship between the multiple water parameters measured along the transect and $p\text{CH}_4$, we calculated 1-min averages from the continuous measurements of T , κ , pH, DO, $f\text{DOM}$ and $p\text{CH}_4$ at the location of the discrete sampling 310 stations in the UP transect. For this analysis, we also included the TOC concentrations from seven stations (average ± 1 std. deviation values are summarized in Table S1), since organic

matter can be a source for methanogens. In addition, we calculated the shortest distance from each station (z_{stas}) and of the navigated transects (z) to any of the river banks and considered this distance as another parameter relevant for the distribution of $p\text{CH}_4$ in the river. The river banks along the navigated transects were digitized in Google Earth Pro®, and no other property was used to define the geographical location of these limits; hence, the river banks are fixed locations without temporal variation for the period of our sampling. We obtained z_{stas} and z from the shortest physical distance between the geographical positions of the sampling stations and of the UP and DOWN transects to any of the defined river banks. The river banks and limits of the transect define the polygonal area of interest for this study (Fig. S2).

To find the correlation between the 1-min averages of $p\text{CH}_4$ and the water properties, as well as the TOC at the sampling stations and z_{stas} , we performed a Pearson pairwise linear correlation analysis ($p < 0.1$).

2.5.2 Random forest regression analysis for extrapolation of transect $p\text{CH}_4$ into a polygonal area of the river section as a function of T , κ and z

We estimated the $p\text{CH}_4$ at the sampling times in the entire river area of a polygon delimited by the river banks and the limits of the navigated transects (Fig. S2). The river bank-forming polygon of the Kolyma River section covered an area of 236.3 km². Within this area we constructed a fine grid regularly distributed within the river polygon and with a horizontal spatial resolution of 0.1 km.

We then built a fine grid polygon in the river for T and κ based on their best fit correlations to z at the transect scale, for the “key sites” and for the “other sites” (depending on the measured $p\text{CH}_4$, T and κ) at the sampling times during the UP and the DOWN transects. The gridded products were used to extrapolate $p\text{CH}_4$ to other areas of the river as defined by the gridded area delimited by the river banks, and on the basis of the highly spatially resolved $p\text{CH}_4$ measured along the transects.

For this, we obtained a best fit between T , κ and z to $p\text{CH}_4$ by applying a random forest regression analysis. First, for “key sites”, this was done as a function of T and κ , i.e., $p\text{CH}_{4_key}(T_{\text{key}}, \kappa_{\text{key}})$. Second, for “other sites” it was done as a function of T , κ and z , i.e., $p\text{CH}_{4_other}(T_{\text{other}}, \kappa_{\text{other}}, z)$. These models were applied to the gridded polygon to extrapolate $p\text{CH}_4$ from the transects to the entire gridded polygon. Once a gridded T and κ was obtained, the corresponding model for $p\text{CH}_{4_key}$ and $p\text{CH}_{4_other}$ was applied. This procedure was done independently for the UP and DOWN data.

3 Results

3.1 Spatial distribution of continuous surface $p\text{CH}_4$ and water properties in UP and DOWN transects

The high-resolution continuous measurements of surface $p\text{CH}_4$ show significant spatial heterogeneity and temporal variability in both the UP and DOWN transects (Fig. 2). Overall, high $p\text{CH}_4$ (up to 46 μatm) was measured in the presence of warm (15.5 °C) and less conductive ($\kappa < 88 \mu\text{S cm}^{-1}$) water, and mostly located closer to the river banks ($z < 1.0 \text{ km}$) (Figs. 3 and 4).

During the UP transect, the average measured $p\text{CH}_4$ was $25.8 \pm 6.7 \mu\text{atm}$ (or in terms of CH_4 concentration, $C_w = 41.5 \pm 9.2 \text{ nmol L}^{-1}$). These values were measured in colder (by 0.6 °C) and less conductive waters (by 16.1 $\mu\text{S cm}^{-1}$) compared to the DOWN transect that was navigated two days later. The DOWN transect had on average 7.4 μatm higher $p\text{CH}_4$ ($33.2 \pm 9.4 \mu\text{atm}$, or $54.3 \pm 14.7 \text{ nmol L}^{-1}$) than the UP transect (Table 1 and Fig. 3). In both transects, the concentration of CH_4 remained supersaturated (by $1189 \pm 198 \%$ in the UP transect and $1622 \pm 380 \%$ in the DOWN transect) with respect to the concentration at atmospheric equilibrium (average $3.2 \pm 0.04 \text{ nmol L}^{-1}$).

The spatial distribution of water properties measured in both transects depicted evident differences between the center of the main stem and the areas at the proximity of banks adjacent to floodplains and at confluences of tributaries with the Kolyma main stem (Fig. 2a and 2b, and supplementary Fig. S3). Specifically, hot spots of $p\text{CH}_4$ with values $> 35 \mu\text{atm}$ were measured in the key sites at the time of the measurements (Figs. 2 and 3).

During the UP transect, the maximum measured $p\text{CH}_4$ was 46.1 μatm at site S5 (Duvannyi Yar), very similar to the value measured during DOWN at the same location (i.e., 44.6 μatm). The maximum $p\text{CH}_4$ measured in the main stem (80.7 μatm) was found at a site halfway along the DOWN transect in a site at the outlet of Leonid's stream (location 68.5281 °N, 160.3437 °E). However, the highest $p\text{CH}_4$ was measured inside streams or tributaries with up to 222.9 μatm at Ambolikha River and up to 92.9 μatm inside Leonid's stream, both navigated during the DOWN transect (Table 1). Larger supersaturations with respect to the atmospheric equilibrium were observed at these two transects with $9610 \pm 403 \%$ in Ambolikha River and $3415 \pm 1051 \%$ in Leonid's stream.

In addition to $p\text{CH}_4$, T and κ were considered to distinguish between the key sites S1 to S5 from the other sites in the river. The key sites S1 to S5 were characterized (besides $p\text{CH}_4 > 37 \mu\text{atm}$) by the presence of warmer ($T > 14.5 \text{ °C}$) and less conductive water ($\kappa < 88 \mu\text{S cm}^{-1}$) at the sampling time. Finally, because the key sites S1 to S5 were evidently located in the

proximity of tributary confluences and banks (i.e., $z < 0.8$ km), we also considered z (distance to the river bank) as a parameter related to high $p\text{CH}_4$ in the main stem (Fig. S2 in supplement). The average, minimum and maximum values of $p\text{CH}_4$, C_w , T , and κ in the UP and DOWN transects at “key sites” and all “other sites” of the transect are summarized in Table 1.

Other areas along the transects where $p\text{CH}_4$ was higher than $37 \mu\text{atm}$ were not included as part of the key sites because their corresponding T or κ did not meet the properties specified above, e.g., at the site of the maximum $p\text{CH}_4$ of $80.7 \mu\text{atm}$ at the outlet of Leonid’s stream where the $T = 15.4^\circ\text{C}$ and $\kappa = 113.1 \mu\text{S cm}^{-1}$ (Figs. 2 and 3).

The pairwise linear correlation analysis ($p < 0.1$) between all the measured parameters showed a statistically significant positive correlation between $p\text{CH}_4$ and T ($r^2 = 0.51$), and a negative correlation to κ ($r^2 = 0.22$), z_{stas} ($r^2 = 0.36$), and DO ($r^2 = 0.17$). No significant correlation was found between $p\text{CH}_4$, $f\text{DOM}$ and turbidity.

To analyze if any of the measured water parameters had an influence on the distribution of $p\text{CH}_4$, we chose the conservative tracers to which CH_4 was significantly correlated: T , κ , and z_{stas} . These conservative parameters are then considered as potential predictors for the presence of dissolved CH_4 in the river, in contrast to reactive tracers such as DO that can be biologically or chemically altered in the river water. The analysis of environmental indicators was done with the continuous high-resolution data only for the main stem areas.

3.2 Influence of conservative tracers on the distribution of riverine $p\text{CH}_4$ along transects and random forest regression as a gap-filling approach

The variations of T and κ in the river are influenced by the proximity to the outlets of tributaries and the riverbanks. This influence is more evident in the UP transect, where T and κ at “key sites” correlated positively with z ($r^2 > 0.45$, $p = 0.05$) (Fig. S4). In the data for the “other sites”, the relation between T and κ vs. z , followed a semi-logarithmic fit ($p = 0.05$) in both the UP and DOWN transects (Fig. S5).

To be able to fill gaps and extrapolate the $p\text{CH}_4$ measured along the transects into the entire polygonal river area, we employed a random forest regression approach based on the correlations between T , κ and z . For this, we first built a fine-gridded polygon for T and κ using the linear (for “key sites”) and semi-logarithmic correlations (for “other sites”) observed at the transect level during the sampling times. Once a gridded T and κ were generated, the corresponding random forest model for $p\text{CH}_{4_key}$ and $p\text{CH}_{4_other}$ at transect level as a function of T , κ and z correspondingly, was applied. This procedure was done independently for the UP and DOWN transects, hence two polygons representing the modeled $p\text{CH}_4$ during 15–16

June 2019 and 16–17 June 2019 were obtained (Fig. S6).

To validate the output of the random forest models, we compared the measured and modeled $p\text{CH}_4$ along each transect. Results show that the skill of the model for the UP transect better reproduces the $p\text{CH}_4$ with an uncertainty of $3.9\ \mu\text{atm}$ than that of the model for the DOWN transect (uncertainty of $9.1\ \mu\text{atm}$) (Fig. S7). A larger error is observed in the areas of the key sites mostly during the DOWN transect.

3.3 Microbial composition and TOC analysis in discrete water samples

Similar to the influences of temperature (T) and specific conductivity (κ) on the distribution of $p\text{CH}_4$, we found that microbial community composition was significantly related to both T ($F = 15.5$, $r^2 = 0.17$, $p < 0.001$) and specific conductivity (κ) ($F = 12.7$, $r^2 = 0.14$, $p < 0.001$) (Fig. 5), while distance to the shore (z) was not significant. The $p\text{CH}_4$ measurements alone explained a low portion of the community variance ($r^2 = 0.06$, $p < 0.03$), and when tested in conjunction with both T and κ , was not a significant contributor to microbial community variance. In this way, microbial community composition can act as a record of $p\text{CH}_4$, as microbes – and T/κ – are less dynamic than $p\text{CH}_4$. Within the context of the strong patterns related to both T and κ , there were spatial patterns that reflected the location within the main stem and the influences of tributaries, with key site S3 (PP20) exhibiting the lowest similarities with the other four key sites and clustering with other water samples collected within the main stem of the river. Conversely, key sites S1 and S2 clustered separately from all other water samples, likely due to the heavy influence of tributary outflow and floodplain inputs (Fig. 5).

Quantifying the 16S rRNA gene abundances of total archaeal and bacterial populations revealed that archaea, were three orders of magnitude lower in abundance than their bacterial counterparts across the river transect. However, the abundances of both were found to strongly correlate (Pearson, $r^2 = 0.81$, $p < 1.8\text{e-}15$) (Supplemental Fig. S8). Within the archaeal 16S sequences detected, we found two putatively methanogenic OTU, each belonging to a different family/genus (*Methanobacteriaceae* – *Methanobacterium*, *Methanoregulaceae* – *Methanoregula*). The highest relative abundance of methanogens (0.012 %) occurred within station PP07 (key site S1) (Fig. 6a), and the other key sites with the highest CH_4 concentrations did not exhibit particularly elevated methanogens abundances. Conversely, bacterial putative groups associated with methanotrophy/methylotrophy, particularly OTU within the family *Methylophilaceae*, were detected at all sites and ranged between 3.5 to 5.5 % relative abundance (Fig. 6b). Restricting our analysis to genera known to be strict methanotrophs, we find sequences affiliated with *Methylobacter* that range from

0.01 – 0.3 % relative abundance, and only traces of *Ca. Methanoperedens* (Supplemental Fig. S9). The relative abundances of these groups were approximated to pseudo-absolute
 450 abundances using the quantitative qPCR results from each sample. Patterns in methanogen abundances were consistent regardless of scale (Fig. 6c), while methano-/methylotrophs exhibited higher abundances within stations PP10, PP11 (key site S2), and PP23-PP25 (incl. key sites S4 and S5), and lower abundances within PP06, PP09, PP15, PP17, and PP20 (key site S3) (Fig. 6d). As this data is based only on DNA analyses, a distinction between active
 455 and dead cells is not possible.

The correlations between the total absolute abundances of archaeal microbial communities against the water properties at stations (Fig. 7) show statistically significant ($p < 0.05$) positive linear correlations between T and the abundance of methanogens ($r^2 = 0.35$, $p = 0.005$) and methano-/methylotrophs ($r^2 = 0.43$, $p = 0.001$) (Figs. 7a and 7b). A statistically significant
 460 negative linear correlation was obtained against κ ($r^2 = 0.31$, $p = 0.007$) for methanogens and for methano-/methylotrophs ($r^2 = 0.24$, $p = 0.02$) (Figs. 7c and 7d). The $p\text{CH}_4$ at stations is also positively correlated and statistically significant (at $p < 0.05$) to the abundance of methano-/methylotrophs ($r^2 = 0.22$, $p = 0.04$), but is not statistically significant when correlated with methanogens (Figs. 7e and 7f).

465 The average TOC measured in 7 out of the 21 sampling stations was $7.5 \pm 0.7 \text{ mg L}^{-1}$ (Table S1). Since organic matter in suspension can be an important carbon source for methanogens, we correlated TOC v $p\text{CH}_4$. A negative but not significant correlation at $p < 0.1$ was found between $p\text{CH}_4$ and TOC.

3.4 Surface CH_4 emissions at transects and polygonal surface area at the Kolyma 470 River section

The average gas transfer velocity during the sampling period was calculated with a hydraulic model ($k_{\text{R12}} = 0.5 \pm 0.02 \text{ m d}^{-1}$) and a wind speed parameterization ($k_{\text{W14}} = 0.4 \pm 0.3 \text{ m d}^{-1}$) are in close agreement. Because the magnitude of the flux density of CH_4 calculated in both transects with these two k values does not differ considerably (i.e., $F_{\text{R12}} = 0.02 \pm 0.007 \text{ mmol m}^{-2} \text{ d}^{-1}$ and $F_{\text{W14}} = 0.01 \pm 0.01 \text{ mmol m}^{-2} \text{ d}^{-1}$), we chose to present only F_{R12} calculated using k_{R12} after the hydraulic model. F_{R12} will be presented hereinafter to as the flux density of CH_4 , FCH_4 .

The average FCH_4 of CH_4 along the UP transect was $0.019 \pm 0.005 \text{ mmol m}^{-2} \text{ d}^{-1}$ and along the DOWN transect was $0.026 \pm 0.008 \text{ mmol m}^{-2} \text{ d}^{-1}$. Maximum FCH_4 values at key sites were
 480 $0.034 \text{ mmol m}^{-2} \text{ d}^{-1}$ for site S5 during the UP transect, and $0.045 \text{ mmol m}^{-2} \text{ d}^{-1}$ at the key site S2 during the DOWN transect (Fig. 3). Average FCH_4 in both transects was 1.5 times higher

at key sites than in the other sites of the transects (Fig. 8). This is relevant considering that the surface area represented by the key sites is 8 to 12 times smaller than the rest of the transects (calculated considering the navigated distance times a radius of 50 m around the sampling point).

The area integrated CH₄ flux in the UP transect (1.27×10^6 m², considering its reach length of 127.7 km times an arbitrary 10 m radius of influence) was 2.4×10^4 mmol d⁻¹. Taking into account only the area of key sites in the UP transect (1.06×10^5 m²) and the emissions in these areas (0.032 mmol m⁻² d⁻¹), the key sites in the UP transect contributed to 14 % ($3,392$ mmol d⁻¹) of the total area integrated emissions in the entire transect. In the DOWN transect, the integrated CH₄ flux was 2.9×10^4 mmol d⁻¹ (area of 1.15×10^6 m², considering 115.4 km of reach length times the 10 m radius). The key sites of the DOWN transect covered an area of 1.37×10^5 m² and the CH₄ emissions in these areas were 0.036 mmol m⁻² d⁻¹, resulting in a contribution of 17 % ($4,932$ mmol d⁻¹) of the total area integrated emissions of the entire DOWN transect.

We also calculated FCH₄ for a smaller stream (Leonid's stream) and the Ambolikha River (second-order tributary of Kolyma River) (Fig. 1), that were navigated during the DOWN transect on 17 June 2019. These navigated sections were not included in our estimate for main channel. The average FCH₄ at the Ambolikha River (0.17 ± 0.008 mmol m⁻² d⁻¹) and at the Leonid's stream (0.05 ± 0.02 mmol m⁻² d⁻¹) were nearly five and two times higher respectively than at the key sites of the main channel during the DOWN transect (Fig. 8).

Based on the modeled *p*CH₄ in the gridded surface area of the Kolyma River section, we calculated the corresponding FCH₄ that would have been emitted through the total surface of the river section (236.3 km²), and not only at the transect locations. The total CH₄ flux at the surface of the river section during the UP transect is calculated as 4.5×10^6 mmol d⁻¹ (or 7.2×10^4 gCH₄ d⁻¹), and for the DOWN transect is 6.1×10^6 mmol d⁻¹ (or 9.8×10^4 gCH₄ d⁻¹) emitted through the surface of the Kolyma River section during the sampling time of both transects (15-17 June 2019).

4 Discussion

4.1 Patterns and indicators of the spatial distribution of CH₄ in Kolyma River and associated tributaries and streams

In June 2019, the Kolyma River exhibited large *p*CH₄ values that were up to 1,300 % supersaturated (equivalent to 28.3 ± 8.5 μatm) with respect to atmospheric equilibrium. These values are comparable to measurements reported for summer in the main channel of the Lena River, i.e., 18 to 51 μatm, calculated from 30 to 85 nmol L⁻¹ for a *T*=14 °C in freshwater;

(Bussmann, 2013). However, a large range in $p\text{CH}_4$ values has been measured in other Arctic Rivers, such that the average $p\text{CH}_4$ in the Kolyma River is three times higher than measurements at the main channel of the Yukon River in North America ($8.4 \mu\text{atm}$) (Striegl et al., 2012), and almost nine times lower than the mean $p\text{CH}_4$ value ($236 \mu\text{atm}$) in surface waters of Kuparuk River in Alaska (Kling et al., 1992).

Our highly spatially-resolved underway continuous measurements of surface dissolved CH_4 were pivotal to reveal spatial variabilities and features in the main river channel that cannot be obtained with sparse discrete sampling. The surface distribution of $p\text{CH}_4$ measured in a ~ 120 km section of Kolyma River was heterogeneous, with nearly two-fold higher concentrations observed along riverbanks and near the confluence of tributaries (69 nmol L^{-1} , or $p\text{CH}_4=41.1 \mu\text{atm}$) than at the central parts of the river (46 nmol L^{-1} , or $p\text{CH}_4=27.8 \mu\text{atm}$) (Fig. 2 and Table 1). Previous studies have demonstrated the influence of land to the distribution of riverine CH_4 concentrations, for example along the Danube River (Canning et al., 2021b), and within the Lena River (Bussmann, 2013). The concentration of dissolved CH_4 in Arctic sites with direct contact to adjacent lands, such as in small tributaries, streams, lakes channels or ponds, has been shown to be two to five times higher than what is observed in the main stems of large rivers (Bussmann, 2013; Dean et al., 2020; Kling et al., 1992; Striegl et al., 2012). In samples from creeks draining from permafrost into the Lena River, CH_4 concentrations (1505 nmol L^{-1} , or $p\text{CH}_4$ of $900 \mu\text{atm}$) were between twenty to fifty times higher than in fluvial waters (Bussmann, 2013). At the Lena Delta, the concentrations of CH_4 are higher (212 nmol L^{-1} , or $p\text{CH}_4$ of $114.7 \mu\text{atm}$, $T=9.8^\circ\text{C}$ and $S=2.45$), because they were directly influenced by bottom soils (Bussmann et al., 2017). In tributaries of the Yukon River, the CH_4 concentrations were up to 690 nmol L^{-1} , being two times higher than in the main stem of the same river (290 nmol L^{-1}) (Striegl et al., 2012). Similarly, our results show that, besides the in-stream variability, tributary or stream CH_4 concentrations measured at the Ambolikha River and Leonid's stream, were between two to six times higher than those in the main channel of Kolyma River.

The average $p\text{CH}_4$ measured at the Ambolikha River ($206.8 \pm 9.8 \mu\text{atm}$) is consistent with the measurements at the Kuparuk River ($236 \mu\text{atm}$) (Striegl et al., 2012), and the mean $p\text{CH}_4$ ($292 \pm 109 \mu\text{atm}$) measured during a 38-day time-series study that started 9 days after the present study (i.e., on 26 June 2019) at a site in the Ambolikha River (Castro-Morales et al., 2022). Whereas the average CH_4 concentration measured at Leonid's stream was $67 \mu\text{atm}$ (111 nM), which is in the same order of magnitude as the maximum value measured at the plume of Kolyma River at the East Siberian Arctic shelf in the summer of 2004 ($55 \mu\text{atm}$,

550 obtained from the reported 110 nM, $T=5\text{ }^{\circ}\text{C}$ and $S=14$) (Shakhova and Semiletov, 2007). We characterized the spatial distribution of riverine $p\text{CH}_4$ as a function of temperature (T), specific conductivity (κ) and the distance from the river banks (z), as suitable indicators for the distribution of CH_4 during the late spring over larger areas of the Kolyma River (and potentially applicable to other Arctic rivers). We found that the distance to river banks is an
555 indicator of the proximity to potential terrestrial CH_4 sources, hence it can be a useful benchmark for understanding the distribution and fate of CH_4 in natural surface waters (Fig. 4). With a statistical approach, we used the selected predictors to fill gaps in areas of the river where no CH_4 data were available (Fig. S6). Similar approaches could be used to improve the CH_4 data currently available for the global CH_4 budget (Saunois et al., 2020) and to aid in
560 forecasting riverine CH_4 following the projected increases in warmer river waters, abrupt permafrost thawing, and collapse of riverbanks.

4.2 Identification of microbial communities associated with the riverine CH_4 concentrations

Overall patterns in microbial community composition, e.g., the similarities in the relative
565 abundances of bacterial and archaeal groups, were also strongly related to the temperature and specific conductivity of the river water (Fig. 5). Unlike with CH_4 , distance to shore was not apparent in explaining differences in community composition. Arctic riverine microbial communities track closely with water temperature, flow rate, and biogeochemistry (Campeau and del Giorgio, 2014; Crump et al., 2009) and match patterns in DOM composition and
570 concentration (Castro-Morales et al., 2022; Kaiser et al., 2017). The strong explanatory power of temperature and specific conductivity we observe in this study fits in with the concept of riverine community coalescence as they approximate the mixing of distinct water sources over a spatially small region, whereby the dynamic community assemblage mechanisms are inextricably linked to transport processes and rapidly changing selective pressures (Mansour
575 et al., 2018). In this sense, spatial patterns in community composition can act as robust bioindicators of the relative inputs of transported metabolic end products derived from terrestrial sources, like CH_4 or CO_2 . To support the relationship between community composition and the originating source of CH_4 , we examined the distributions of functional microbial groups putatively associated with CH_4 production and consumption. The strongest
580 evidence was the overlap in detected methanotrophs and methanogens within our study and a previous study by Kwon et al. (2017), that examined these groups within permafrost soils adjacent to our site (PP09). More specifically the highest relative abundances of groups associated with *Methanobacterium* and *Methylobacter* in both the surficial soils and our

discrete water samples.

585 Expanding on this, biological CH₄ production has traditionally been assumed to occur only in anoxic environments, and methanogens as strict anaerobes, are unsuited to grow within oxic river waters. Our data shows that river water was oxic at all stations with an average O₂ saturation of 110 %, which should preclude methanogenesis. However, there is increasing evidence that there is CH₄ production in oxic marine and freshwaters, and a link between oxic
590 *in situ* production of CH₄ and algal dynamics (i.e., photosynthesis and respiration rates) (Bogard et al., 2014). Oversaturation of CH₄ in oxic surface waters of lakes can also result from CH₄ release from littoral sediments in combination with horizontal transport to the open water. The relative importance of both processes is under debate (Bogard et al., 2014; Encinas Fernández et al., 2016; Grossart et al., 2011; Peeters and Hofmann, 2021). The second
595 process also explains better the higher CH₄ concentrations observed in shallow zones compared to deep waters of lakes (Peeters and Hofmann, 2021). For the Kolyma River, we propose that the oversaturated CH₄ concentrations located close to the river bank and at confluences with tributaries, and the presence of methanogens, is mainly caused by the lateral release of CH₄-rich pore water and soil-borne methanogens. This process might be dominant
600 during permafrost melting and resuspension events, rather than *in situ* net production of CH₄ in oxic surface waters by active methanogens. The relative and pseudo-absolute abundances of sequences affiliated with methanogens further act as more specific indicators of sources originating from anoxic, terrestrial CH₄ hotspots, as supported by the statistically significant correlation between methanogen abundance and CH₄ concentration (Fig. 7). Additionally, we
605 anticipate that the methanogenic archaea exhibit longer residence times than CH₄ itself due to its high diffusion and oxidation rates. The presence of soil-derived methanogens in the river water might be indicative of even higher riverine CH₄ concentrations, as part of it can be already outgassed or oxidized. The weaker correlation of CH₄ to methanogen abundance compared to temperature or specific conductivity, parameters expected to change slower than
610 CH₄ concentrations, likely reflects these differences in transport mechanisms. Of the two methanogens we detected, *Methanobacterium* was recently shown to be the primary methanogen detected in the surface waters of thermokarst ponds and is more typical of acidic and peat-dominated aquatic ecosystems (Vigneron et al., 2019). *Methanoregula* (within order *Methanomicrobiales*) have also been shown to be abundant groups within permafrost thaw
615 lakes (Crevecoeur et al., 2016) and were suggested to be more typical of deeper and less acidic water bodies (Vigneron et al., 2019) (Fig. 6).
Conversely, we expected microbial groups that consume CH₄ to also be indicative of CH₄

sources into the river. Groups affiliated with methylotrophy (e.g., *Methylophilaceae* – *Methylotenera*) exhibited ten times higher relative abundances than groups of strict methanotrophic organisms (*Methylobacter*) (Fig. 6), suggesting that in addition to CH₄, other sources like methanol associated to the degradation of CO₂ by methanotrophs (Xin et al., 2007) or by some groups of phytoplankton (Mincer and Aicher, 2016), were sources of carbon in this environment. In support of this finding, aerobic methanotrophs have been found at much higher relative abundances (>25 %) and higher diversity within thermokarst well-stratified subarctic Canadian ponds, than the maximum of 0.3 % detected here, where distinct genera (*Methylobacter* and *Methylomonas*) within the order *Methylococcales* where the most abundant (Crevecoeur et al., 2015; Vigneron et al., 2019). This is a sensical finding, as the dynamic river flow enables the diffusive CH₄ transport and emissions to the atmosphere compared to the emissions across smaller surface areas in highly-stratified, less dynamic and largely anoxic pond environments. The majority of the CH₄ produced in thawing permafrost is first locally oxidized before it can be released to the atmosphere (Olid et al., 2021). Thus, the higher relative abundance of CH₄-consuming bacteria compared to CH₄-producing archaea in the Kolyma River suggests that a considerable fraction of CH₄ is already oxidized within the recently thawed active layer.

4.3 Temporal variability of CH₄ in Kolyma River

Our continuous high-resolution measurements of *p*CH₄ in the Kolyma River allowed us also to identify a large temporal variability in spite of the short time scale of our measurements. The differences in the *p*CH₄ and FCH₄ (flux density of CH₄) between the UP and DOWN transects might be due to a rapid response to changes in CH₄ driven by the interactions between the main flow of the river and the continuous contribution of external CH₄ inputs resulting from melting, rather than by an advective signal travelling down the main channel of Kolyma River. Still, our measurements cannot represent any mid- to long-term CH₄ variation in the river, and the differences between the transects might also be due to different spatial locations.

The Kolyma River Basin is the only one in the Arctic completely underlain by continuous permafrost, which could result in even higher soil CH₄ production and release into the river network during permafrost thaw compared to other Arctic rivers. During the Arctic melt season (May to June), the surface hydrologic connectivity between the land and rivers is enhanced. As the seasonal progression takes place, deeper water-saturated soil layers are thawed, and substances, microorganisms, and gases, like CH₄, are mobilized through the lateral transfer from groundwater discharge into Arctic inland waters, particularly to the

fluvial network (Connolly et al., 2020; Harms et al., 2020; Saunois et al., 2020). It has been demonstrated that the majority of the CH₄ emitted to the atmosphere from subarctic ponds is sustained by the discharge of CH₄ from groundwaters upon the active layer thaw (Olid et al., 2021).

4.4 CH₄ emissions in Kolyma River and comparison to other estimates

The average estimated annual flux in the polygon section at the Kolyma River during our sampling is 1.24×10^7 g CH₄ taking into account a polygon surface area of 236.3 km² and 146-days ice-free season (between 20th May and 12th October 2019 obtained from the river discharge curve, Fig. S1). This calculation is by far from robust and largely uncertain, considering that our measurements only correspond to a short-term data set during the open water season, and that large temporal and spatial variations in relation to e.g., changes in water sources, temperature regime and lateral carbon inputs throughout the ice-free period is expected. This has been recently demonstrated at the Ambolikha River (tributary of the Kolyma River), where riverine CH₄ concentrations decreased over time during the open water season due to persistent emissions to the atmosphere dominating over declining external gas inputs during the summer low flow (Castro-Morales et al., 2022). Thus, the annual CH₄ flux value provided here for the investigated Kolyma River section, provides an upper end of the potential magnitude and relevance of CH₄ atmospheric emissions from an Arctic River.

Despite the large uncertainty, our estimated CH₄ emissions are four orders of magnitude smaller than the annual flux of CH₄ at the East Siberian Arctic Shelf (ESAS) estimated to be 0.11×10^{12} g CH₄ yr⁻¹ (or 0.11 Tg CH₄ yr⁻¹, for a 90-days ice-free season) in summer of 2003 and 2004 for a surface area of 1.0×10^6 km² (which is orders of magnitude greater than the polygon section of Kolyma River) (Shakhova and Semiletov, 2007). In Arctic shelves, the concentration of CH₄ is strongly influenced by riverine inputs, particularly in bottom layers of shelf waters due to differential water density gradients (Shakhova and Semiletov, 2007). Decreasing flow velocities (i.e., discharge) allow the sedimentation of organic matter in the delta areas, stimulating microbial sedimentary processes that finally lead to the formation of CH₄ and CO₂. Dropping water levels during summer also facilitates CH₄ emissions from riverine sediments to the atmosphere. This has been observed in the Lena River region, where contributions from bottom surface sediments are more significant to the measured CH₄ concentrations than riverine lateral exports (Bussmann et al., 2017).

As both the oxidation rates and the diffusive emissions of CH₄ through the water-atmosphere interface are faster processes than the lateral gas transport in the water column. Thus, despite the large CH₄ concentrations and emissions identified in the upstream river waters, the surface

riverine CH₄ measured >100 km upstream of the shelf is locally emitted (or oxidized) and does not influence the surface CH₄ concentrations measured at the river plume and at the East Siberian Arctic Shelf.

Morphology and stream size seem to be also key parameters for the amount of gas delivered from land and emitted through the water surface into the atmosphere, as the potential for large gas emissions is higher in smaller streams with shorter water travel distances. Our data support this assumption, as the FCH₄ at key sites was two to five times lower than the average FCH₄ at the smaller Leonid's stream and Ambolikha River respectively (Fig. 8). The surface areas of the key sites characterized by elevated FCH₄ are between 8 to 12 times smaller than the surface area covered by the rest of the transect. However, the CH₄ emissions at key sites were 1.5 times higher than in the other sites, and represent between 13 to 20 % of the total cumulative emissions in both transects.

Because the diffusion of CH₄ in water is slower than in air, riverbanks can thus act as efficient vectors for the local emissions of CH₄ formed and stored in the subsoil. The projected increase in freshwater inputs, deepening of active layers, and increase in soil drainage, as more permafrost is thawing in response to warmer and wetter Arctic summers (AMAP, 2017; Bring et al., 2016; Bussmann et al., 2017; Chiasson-Poirier et al., 2020), will enhance the input of CH₄ from external terrestrial sources at hotspots over extended periods during the open water season. Additionally, projected longer ice-free periods in the Arctic, i.e., an earlier start of melt periods and longer open water seasons, can therefore lead to an increase in CH₄ emissions from inland waters (Wik et al., 2016). This ultimately will have an impact on the current CH₄ budget of the Arctic. By not considering the variable aquatic ecosystems and water cycle of the Arctic, the estimated 4 to 5 % contribution of high latitudes to the total global CH₄ emissions (Rosentreter et al., 2021; Saunois et al., 2020) may be underestimated.

The irregular location of CH₄ hot spots along the river banks and their potentially continuous elevated CH₄ contributions to the river, possess a challenge to estimating lateral transport of CH₄ from upstream to downstream waters. Elevated CH₄ concentrations at the Arctic shelves are thus primarily influenced by local sources (i.e., bottom soils and degrading shelves) (Shakhova and Semiletov, 2007). However, to improve the estimates of riverine CH₄ concentrations that can actually reach the ocean in the context of increasing warming and thawing, and to improve the knowledge of the contribution of Arctic rivers and streams to the regional and global CH₄ budgets, it is necessary to intensify the spatial and temporal resolution of the direct measurements of CH₄ in Arctic Rivers.

5 Conclusions

In this study, we measured for the first time continuous high-resolution $p\text{CH}_4$ in a large section of Kolyma River during the late freshet of 2019, and combined these observations with microbial community analysis in water samples to investigate the potential source of this gas. The large spatial variability of surface CH_4 concentrations in the river channel was associated with hotspots located at the river bank and at confluences with tributaries where CH_4 was almost two times higher than at the center of the channel. The identified presence of CH_4 -producing archaea in a well oxygenated river water suggests that most of the CH_4 is laterally transported from external terrestrial sources into the river channel, rather than produced within the river water. Elevated riverine local CH_4 emissions were associated with identified hotspot areas on land suggesting efficient linkages between the land and the aquatic ecosystems. Our analysis does not reveal the reach length of the CH_4 measured from our site to downstream waters. We suggest that the CH_4 measured in waters 100 km upstream the Arctic Ocean, might not reach shelf waters and instead is locally emitted to the atmosphere or oxidized in the river course. For this specific purpose, future works should include stable isotope studies to trace the sources and pathways of the CH_4 in the river water. Without continuous measurements, it will remain unclear how much CH_4 is actually transported and emitted at the peak of the melt period at the highest annual river discharge. As rivers and ocean shelves in the Arctic experience more abrupt collapses, erosion and thawing, this may contribute to the liberation and transport of soil-derived CH_4 , resulting in the expansion of key areas and an increase in CH_4 emissions into the atmosphere. Our results provide a glimpse of the potential contribution of CH_4 emissions from Arctic Rivers, adding up to the largely unknown contributions from permafrost and inland waters.

Data availability

The hydrologic and gas data presented in this work will be made available through a link to the Zenodo public repository upon the publication of this work. All sequences of the microbial data have been deposited in GenBank with the reference BioProject No. PRJNA881395.

Competing interests

The authors declare that they have no conflict of interest

Author contribution

755 K.C.-M. conceived and designed the study. K.C.-M, A.C., A.K., K.K., S.A., O.K. and N.Z. contributed to fieldwork and logistics. K.C.-M, A.C., M.G., S.A., W.A.O. contributed to lab work, sample and data analyses. K.C.-M., A.C. and W.A.O wrote the paper with contributions from all authors in draft versions prior to submission.

Acknowledgments

760 This work was conceived within the project PROPERAQUA funded by the Deutsche Forschungsgemeinschaft (DFG, German Research Foundation) (project No. 396657413). The contributions from AC and AK were funded by the MOSES program of the Helmholtz Association and the C-CASCADES ITN of the EU (project No. 643052). KK and WAO were supported by the Collaborative Research Centre 1076 AquaDiva (CRC AquaDiva) funded by 765 DFG (project No. ID 218627073). MG and OK were supported through funding by the European Commission (INTAROS project, H2020-BG-09-2016, Grant Agreement No. 727890, Nunataryuk project, H2020-BG-11-2016/17, Grant Agreement No. 773421). Especial thanks to the Northeast Scientific Station and the Pleistocene Park in Chersky for 770 their invaluable assistance during fieldwork. Thanks to Dr. Robert Lehmann for the analysis of TOC samples at the FSU-Jena.

References

- AMAP, Snow, water, ice and permafrost in the Arctic (SWIPA), In, Oslo, Norway, 269,
775 2017.
- Amorocho, J. and Devries, J. J.: A new evaluation of the wind stress coefficient over water surfaces, *Journal of Geophysical Research*, 85, 433-442, 10.1029/JC085iC01p00433, 1980.
- Bogard, J. M., del Giorgio, P. A., Boutet, L., Garcia Chavez, M. C., Prairie, Y. T., Merante, A., and Derry, A. M.: Oxic water column methanogenesis as major component of aquatic CH₄ fluxes, *Nature Communications*, 5, 5250, 10.1038/ncomms6350, 2014.
780
- Bring, A., Fedorova, I., Dibike, Y., Hinzman, L., Mård, J., Mernild, S. H., Prowse, T. D., Semenova, O., Stuefer, S. L., and Woo, M.-K.: Arctic terrestrial hydrology: a synthesis of processes, regional effects, and research challenges, *Journal of Geophysical Research: Biogeosciences*, 121, 621-649, 10.1002/2015JG003131, 2016.
- 785 Bussmann, I.: Distribution of methane in the Lena Delta and Buor-Khaya Bay, Russia, *Biogeosciences*, 10, 4641-4652, 10.5194/bg-10-4641-2013, 2013.
- Bussmann, I., Hackbusch, S., Schaal, P., and Wichels, A.: Methane distribution and oxidation around the Lena Delta in summer 2013, *Biogeosciences*, 14, 4985-5002, 10.5194/bg-14-4985-2017, 2017.
- 790 Campeau, A. and del Giorgio, P. A.: Patterns in CH₄ and CO₂ concentrations across boreal rivers: major drivers and implications for fluvial greenhouse emissions under climate change scenarios, *Global Change Biology*, 20, 1075-1088, 10.1111/gcb.12479, 2014.
- Canning, A., Körtzinger, A., Fietzek, P., and Rehder, G.: Technical note: seamless gas measurements across Land-Ocean Aquatic Continuum - corrections and evaluation of sensor data for CO₂, CH₄ and O₂ from field deployments in contrasting environments,
795 *Biogeosciences*, 18, 1351-1373, 10.5194/bg-18-1351-2021, 2021a.
- Canning, A., Wehrli, B., and Körtzinger, A.: Methane in the Danube Delta: the importance of spatial patterns and diel cycles for atmospheric emissions estimates, *Biogeosciences*, 18, 3961-3979, 10.5194/bg-18-3961-2021, 2021b.
- 800 Castro-Morales, K., Canning, A., Körtzinger, A., Göckede, M., Küsel, K., Overholt, W. A., Wichard, T., Redlich, S., Arzberger, S., Kolle, O., and Zimov, N.: Effects of reversal of water flow in an Arctic stream on fluvial emissions of CO₂ and CH₄, *Journal of Geophysical Research: Biogeosciences*, 127, e2021JG006485, 10.1029/2021JG006485, 2022.
- 805 Charkin, A. N., M., R. v. d. L., Shakhova, N. E., Gustafsson, Ö., Dudarev, O. V., Cherepnev, M. S., Salyuk, A. N., Koshurnikov, A. V., Spivak, E. A., Gunar, A. Y., Ruban, A. S., and Semiletov, I. P.: Discovery and characterization of submarine groundwater discharge in the Siberian Arctic seas: a case study in the Buor-Khaya Gulf, Laptev Sea, *The Cryosphere*, 11, 2305-2327, 10.5194/tc-11-2305-2017, 2017.
- 810 Chiasson-Poirier, G., Franssen, J., Lafrenière, M. J., Fortier, D., and Lamoureux, S. F.: Seasonal evolution of active layer thaw depth and hillslope-stream connectivity in a permafrost watershed, *Water Resources Research*, 56, 10.1029/2019WR025828, 2020.
- Connolly, C. T., Cardenas, M. B., Burkart, G. A., Spencer, R. G. M., and McClelland, J. W.:

- Groundwater as a major source of dissolved organic matter to Arctic coastal waters, *Nature Communications*, 11, 1-8, 10.1038/s41467-020-15250-8, 2020.
- 815 Crevecoeur, S., Vincent, W. F., Comte, J., and Lovejoy, C.: Bacterial community structure across environmental gradients in permafrost thaw ponds: methanotroph-rich ecosystems, *Frontiers in Microbiology*, 6, 192, 10.3389/fmicb.2015.00192, 2015.
- Crevecoeur, S., Vincent, W. F., and Lovejoy, C.: Environmental selection of planktonic methanogens in permafrost thaw ponds, *Scientific Reports*, 6, 31312, 10.1038/srep31312, 820 2016.
- Crump, B. C., Peterson, B. J., Raymond, P. A., Amon, R. M. W., Rinehart, A., McClelland, J. W., and Holmes, R. M.: Circumpolar synchrony in big river bacterioplankton, *Proceedings of the National Academy of Sciences of the United States of America*, 106, 10.1073/pnas.0906149106, 2009.
- 825 Dabrowski, J. S., Charette, M. A., Mann, P. J., Ludwig, S. M., Natali, S. M., Holmes, R. M., Schade, J. D., Powell, M., and Henderson, P. B.: Using radon to quantify groundwater discharge and methane fluxes to a shallow, tundra lake on the Yukon Kuskokwim Delta, Alaska, *Biogeochemistry*, 148, 69-89, 10.1007/s10533-020-00647-w, 2020.
- Dean, J. F., Meisel, O. H., Martyn, R. M., Belelli, L. M., Garnett, M. H., Lenderink, H., van Logtestijn, R., Borges, A. V., Bouillon, S., Lambert, T., Röckmann, T., Maximov, T., Petrov, R., Karsanaev, S., Aerts, R., van Huissteden, J., Vonk, J. E., and Dolman, A. J.: East Siberian Arctic inland waters emit mostly contemporary carbon, *Nature Communications*, 11, 1627, 830 10.1038/s41467-020-15511-6, 2020.
- Dean, J. F., Middelburg, J. J., Röckmann, T., Aerts, R., Blauw, L. G., Egger, M., Jetten, M. S. M., de Jong, A. E. E., Meisel, O. H., Rasigraf, O., Slomp, C. P., in't Zandt, M. H., and Dolman, A. J.: Methane feedbacks to the global climate system in a warmer world, *Reviews of Geophysics*, 56, 1-44, 10.1002/2017RG000559, 835 2018.
- Dlugokencky, E. and Tans, P. P.: www.esrl.noaa.gov/gmd/ccgg/trends/, 2020.
- Downing, B. D., Pellerin, B. A., Bergamaschi, B. A., Saraceno, J. F., and Kraus, T. E. C.: 840 Seeing the light: the effects of particles, dissolved materials, and temperature on in situ measurements of DOM fluorescence in rivers and streams, *Limnology and Oceanography: Methods*, 10, 767-775, 10.4319/lom.2012.10.767, 2012.
- Encinas Fernández, J., Peeters, F., and Hofmann, H.: On the methane paradox: transport from shallow water zones rather than in situ methanogenesis is the major source of CH₄ in the open 845 surface water of lakes, *Journal of Geophysical Research: Biogeosciences*, 121, 2717-2726, 10.1002/2016JG003586, 2016.
- Etminan, M., Myhre, G., Highwood, E. J., and Shine, K. P.: Radiative forcing of carbon dioxide, methane, and nitrous oxide: a significant revision of the methane radiative forcing, *Geophysical Research Letters*, 43, 12614-12623, 10.1002/2016GL071930, 2016.
- 850 Grossart, H.-P., Frindte, K., Dziallas, C., Eckert, W., and Tang, K. W.: Microbial methane production in oxygenated water column of an oligotrophic lake, *Proceedings of the National Academy of Sciences of the United States of America*, 108, 19657-19661, 10.1073/pnas.1110716108, 2011.

- 855 Harms, T. K., Rocher-Ros, G., and Goodsey, S. E.: Emission of greenhouse gases from water tracks draining Arctic hillslopes, *Journal of Geophysical Research: Biogeosciences*, 125, e2020JG005889, 10.1029/2020JG005889, 2020.
- IPCC, Climate Change 2014: Synthesis Report. Contribution of Working Groups I, II and III to the Fifth Assessment Report of the Intergovernmental Panel on Climate Change, In, Geneva, Switzerland, 151, 2014.
- 860 Kaiser, K., Canedo-Oropeza, M., McMachon, R., and Amon, R. M. W.: Origins and transformations of dissolved organic matter in large Arctic rivers, *Scientific Reports*, 7, 1-11, 10.1038/s41598-017-12729-1, 2017.
- 865 Karlsson, J., Serikova, S., Vorobyev, S. N., Rocher-Ros, G., Denfeld, B. A., and Pokrovsky, O. S.: Carbon emission from Western Siberian inland waters, *Nature Communications*, 12, 1-8, 10.1038/S41467-021-21054-1, 2021.
- Kling, G. W., Kipphut, G. W., and Miller, M. C.: The flux of CO₂ and CH₄ from lakes and rivers in arctic Alaska, *Hydrobiologia*, 240, 23-26, 10.1007/BF00013449, 1992.
- 870 Kwon, M. J., Beulig, F., Ilie, I., Wildner, M., Küsel, K., Merbold, L., Mahecha, M. D., Zimov, N., Zimov, S., Heimann, M., Schuur, E. A., Kostka, J. E., Kolle, O., Hilke, I., and Göckede, M.: Plants, microorganisms, and soil temperatures contribute to a decrease in methane fluxes on a drained Arctic floodplain, *Global Change Biology*, 23, 2396-2412, 10.1111/gcb.13558, 2017.
- 875 Lammers, R. B., Shiklomanov, A. I., Vörösmarty, C. J., Fekete, B. M., and Peterson, B. J.: Assessment of contemporary Arctic river runoff based on observational discharge records, *Journal of Geophysical Research*, 106, 3321-3334, 10.1029/2000JD900444, 2001.
- 880 Mann, P. J., Strauss, J., Palmtag, J., Dowdy, K., Ogneva, O., Fuchs, M., Bedington, M., Torres, R., Polimene, L., Overduin, P. P., Mollenhauer, G., Grosse, G., Rachold, V., Sobczak, W. V., Spencer, R. G. M., and Juhls, B.: Degrading permafrost river catchments and their impact on Arctic Ocean nearshore processes, *Ambio*, 51, 439-455, 10.1007/s13280-021-01666-z, 2022.
- Mansour, I., Heppell, C. M., Ryo, M., and Rilling, M. C.: Application of the microbial community coalescence concept to riverine networks, *Biological Reviews of the Cambridge Philosophical Society*, 93, 1832-1845, 10.1111/brv.12422, 2018.
- 885 Mincer, T. J. and Aicher, A. C.: Methanol production by a broad phylogenetic array of marine phytoplankton, *PLoS ONE*, 11, e0150820, 10.1371/journal.pone.0150820, 2016.
- Olefeldt, D., Turetsky, M. R., Crill, P. M., and McGuire, A. D.: Environmental and physical controls on northern terrestrial methane emissions across permafrost zones, *Global Change Biology*, 19, 589-603, 10.1111/gcb.12071, 2013.
- 890 Olid, C., Zannella, A., and Lau, D. C. P.: The role of methane transport from the active layer in sustaining methane emissions and food chains in subarctic ponds, *Journal of Geophysical Research: Biogeosciences*, 126, e2020JG005810, 10.1029/2020JG005810, 2021.
- Peeters, F. and Hofmann, H.: Oxidic methanogenesis is only a minor source of lake-wide diffusive CH₄ emissions from lakes, *Nature Communications*, 12, 1206, 10.1038/s41467-021-21215-2, 2021.

- 895 Raymond, P. A., Zappa, C. J., Butman, D., Bott, T. L., Potter, J. D., Mulholland, P., Laursen, E., McDowell, W. H., and Newbold, D.: Scaling the gas transfer velocity and hydraulic geometry in streams and small rivers, *Limnology and Oceanography: fluids and environments*, 2, 41-53, 10.1215/21573689-1597669, 2012.
- 900 Rosentreter, J. A., Borges, A. V., Deemer, B. R., Holgerson, M. A., Liu, S., Song, C., Melack, J. M., Raymond, P. A., Duarte, C. M., Allen, G. H., Olefeldt, D., Poulter, B., Battin, T. I., and Eyre, D.: Half of global methane emissions come from highly variable aquatic ecosystem sources, *Nature Geoscience*, 14, 225-230, 10.1038/s41561-021-00715-2, 2021.
- 905 Saunois, M., Stavert, A. R., Bousquet, P., Canadell, J. G., and et al.: The global methane budget 2000-2017, *Earth System Scientific Data*, 12, 1561-1623, 10.5194/essd-12-1561-2020, 2020.
- Schuur, E. A., McGuire, D., Schädel, C., Grosse, G., Harden, J. W., Hayes, D. J., Hugelius, G., Koven, C. D., Kuhry, P., Lawrence, D. M., Natali, S. M., Olefeldt, D., Romanovsky, V. E., Schaefer, K., Turetsky, M. R., Treat, C. C., and Vonk, J. E.: Climate change and the permafrost carbon feedback, *Nature*, 520, 171-179, 10.1038/nature14338, 2015.
- 910 Shakhova, N. and Semiletov, I. P.: Methane release and coastal environment in the East Siberian Arctic shelf, *Journal of Marine Systems*, 66, 227-243, 10.1016/j.jmarsys.2006.06.006, 2007.
- 915 Shakirov, R. B., Mau, S., Mishukova, G. I., Obzhairov, A. I., Shakirova, M. V., and Mishukova, O. V.: The features of methane fluxes in the western and eastern Arctic: a review. Part I, *Geosystems of Transition Zones*, 4, 004-025, 10.30730/2541-8912.2020.4.1.004-025, 2020.
- Snyder, L., Potter, J. D., and McDowell, W. H.: An evaluation of nitrate, fDOM, and turbidity sensors in New Hampshire Streams, *Water Resources Research*, 54, 2466-2479, 10.1002/2017WR020678, 2018.
- 920 Stanley, E. H., Casson, N. J., Christel, S. T., Crawford, J. T., Loken, L. C., and Oliver, S. K.: The ecology of methane in streams and rivers: patterns, controls, and global significance, *Ecological Monographs*, 86, 146-171, 10.1890/15-1027, 2016.
- 925 Striegl, R. G., Dornblaser, M. M., McDonald, C. P., Rover, J. R., and Stets, E. G.: Carbon dioxide and methane emissions from the Yukon River System, *Global Biogeochemical Cycles*, 26, GB0E05, 10.1029/2012GB004306, 2012.
- Turetsky, M. R., Abbott, B. W., Jones, M. C., Walter Anthony, K., Olefeldt, D., Schuur, E. A., Grosse, G., Kuhry, P., Hugelius, G., Koven, C., Lawrence, D. M., Gibson, C., Sannel, A. B., and McGuire, D.: Carbon release through abrupt permafrost thaw, *Nature Geoscience*, 13, 138-143, 10.1038/s41561-019-0526-0, 2020.
- 930 Vigneron, A., Cruaud, P., Bhiry, N., Lovejoy, C., and Vincent, W. F.: Microbial community structure and methane cycling potential along a thermokarst pond-peatland continuum, *Microorganisms*, 7, 10.3390/microorganisms7110486, 2019.
- 935 Vorobyev, S. N., Karlsson, J., Kolesnichenko, Y. Y., and Koretz, M.: Fluvial carbon dioxide emission from the Lena River basin during spring flood, *Biogeosciences Discussions*, doi: 10.5194/bg-2021-109, 2021. 10.5194/bg-2021-109, 2021.

- Wanninkhof, R.: Relationship between gas exchange and wind speed over the ocean, *Journal of Geophysical Research*, 97, 7373-7381, 10.1029/92JC00188, 1992.
- Wanninkhof, R.: Relationship between wind speed and gas exchange over the ocean revisited, *Limnology and Oceanography: Methods*, 12, 351-362, 10.4319/lom.2014.12.351, 2014.
- 940 Watras, C. J., Hanson, P. C., Stacy, T. L., Morrison, K. M., Mather, J., Hu, Y.-H., and Milewski, P.: A temperature compensation method for CDOM fluorescence sensors in freshwater, *Limnology and Oceanography Methods*, 9, 296-301, 10.4319/lom.2011.9.296, 2011.
- 945 Weiss, R. F.: The solubility of nitrogen, oxygen and argon in water and sea water, *Deep Sea Research*, 17, 721-735, 10.1016/0011-7471(70)90037-9, 1970.
- Wiesenburg, D. A. and Guinasso, J. N. L.: Equilibrium solubilities of methane, carbon monoxide, and hydrogen in water and sea water, *Journal of Chemical and Engineering Data*, 24, 356-360, 10.1021/cr60306a003, 1979.
- 950 Wik, M., Varner, R. K., Walter Anthony, K., MacIntyre, S., and Bastviken, D.: Climate-sensitive northern lakes and ponds are critical components of methane release, *Nature Geoscience*, 99-106, 10.1038/NGEO2578, 2016.
- Xin, J., Zhang, Y., Zhang, S., Xia, C., and Li, S.: Methanol production from CO₂ by resting cells of the methanotrophic bacterium *Methylosinus trichosporium* IMV 3011, *Journal of Basic Microbiology*, 47, 426-435, 10.1002/jobm.200710313, 2007.
- 955 Zolkos, S., Tank, S. E., Striegl, R., and Kokelj, S. V.: Thermokarst effects on carbon dioxide and methane fluxes in streams on the Peel Plateau (NWT, Canada), *Journal of Geophysical Research: Biogeosciences*, 124, 1781-1798, 10.1029/2019JG005038, 2019.

Figure Captions

Figure 1 – Navigated transects in the Kolyma River: upstream (UP) (grey line, sampled from 15 June 2019 at 12:30 h to 16 June 2019 at 16:59 h) and downstream (DOWN) (black line, navigated on 16-17 June 2019). Gaps in the continuous UP and DOWN transects are data not considered for the analysis because they involved navigation outside the main river channel (i.e., transects at Leonid's stream and the Ambolikha River indicated in red). Discrete samples were collected in 21 sampling stations (PP05-PP25) during the UP transect (grey markers). Key sites (and stations): S1 (PP07), S2 (PP11), S3 (PP20), S4 (PP23), and S5 (PP25) are circled in yellow. This map was created using MATLAB® with data from a composite image for June, July and August from 2005-2018 using Sentinel-2 NDVI maps (<https://developers.google.com/earth-engine/datasets/catalog/sentinel>).

Figure 2 – Spatial distribution of water properties measured along transects UP (left) and DOWN (right) at the main stem of the Kolyma River for $p\text{CH}_4$ (a and b), T (c and d), and κ (e and f). The location of key sites S1 to S5 are indicated. The values corresponding to Ambolikha River and Leonid's stream are not shown.

Figure 3 – Water properties measured in transects UP (grey) and DOWN (black): a) water temperature, T ; b) water-specific conductivity, κ ; c) CH_4 concentration, C_w , and d) flux density of CH_4 , FCH_4 , all shown as a function of the navigated distance (km) along each transect. The location corresponding to the key sites S1 to S5 are indicated and color-coded in each signal (light grey – UP transect and black – DOWN transect). The Ambolikha River and Leonid's stream are shown in red. Gaps in the data indicate erroneous or not measured data in the transect.

Figure 4 – Correlation graphs for UP (a and b) and DOWN (c and d) transects between T , κ and $p\text{CH}_4$ as a function of the distance to bank (z in km) indicated in the color scale.

Figure 5 – Riverine microbial community composition linked to temperature (left) and specific conductivity (right). Both plots represent the same underlying community data, with dissimilarities determined by the Bray-Curtis metric and visualized with non-metric multidimensional scaling plots.

Figure 6 – Relative (top) and pseudo-absolute (bottom) abundances of putatively methanogenic archaeal genera (left) and methylotrophic bacterial families (right). An expanded version that includes only the methanotrophs is available in the supplemental information.

Figure 7 – Linear correlations between the total absolute abundances of archaeal microbial communities (left, methanogens and right, methanotrophs) and the 1-min averages of water properties measured at the 21 sampling stations along the DOWN transect in Kolyma River. Red numbers in some of the markers indicate the station number corresponding to the key sites S1 to S5.

Figure 8 – Average flux density of CH_4 (FCH_4) calculated for the entire UP and DOWN transects, and for the key sites and other sites. FCH_4 for the tributaries Ambolikha River and Leonid's stream are also shown. Error bars denote the standard deviation of the mean.

Figures

Fig. 1

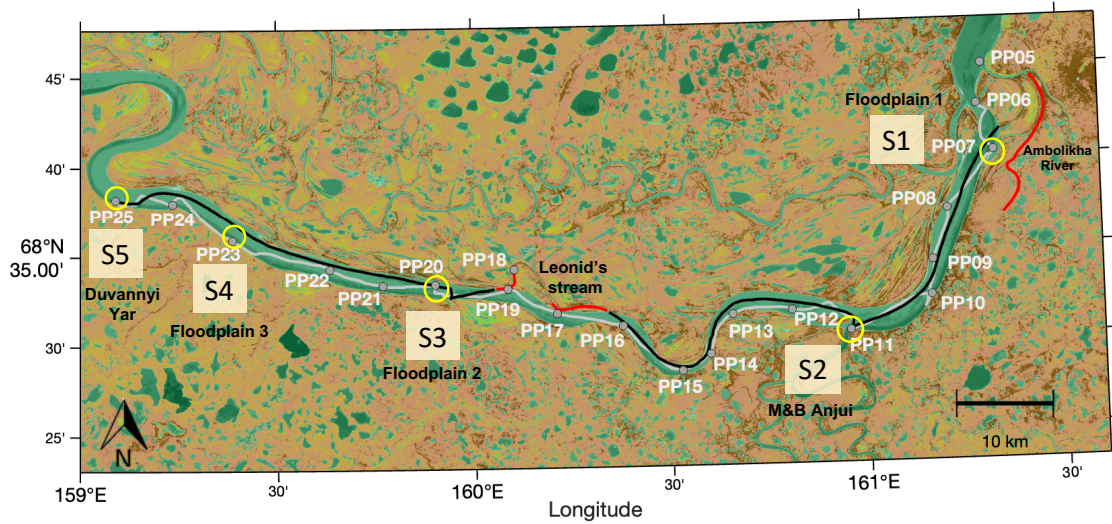
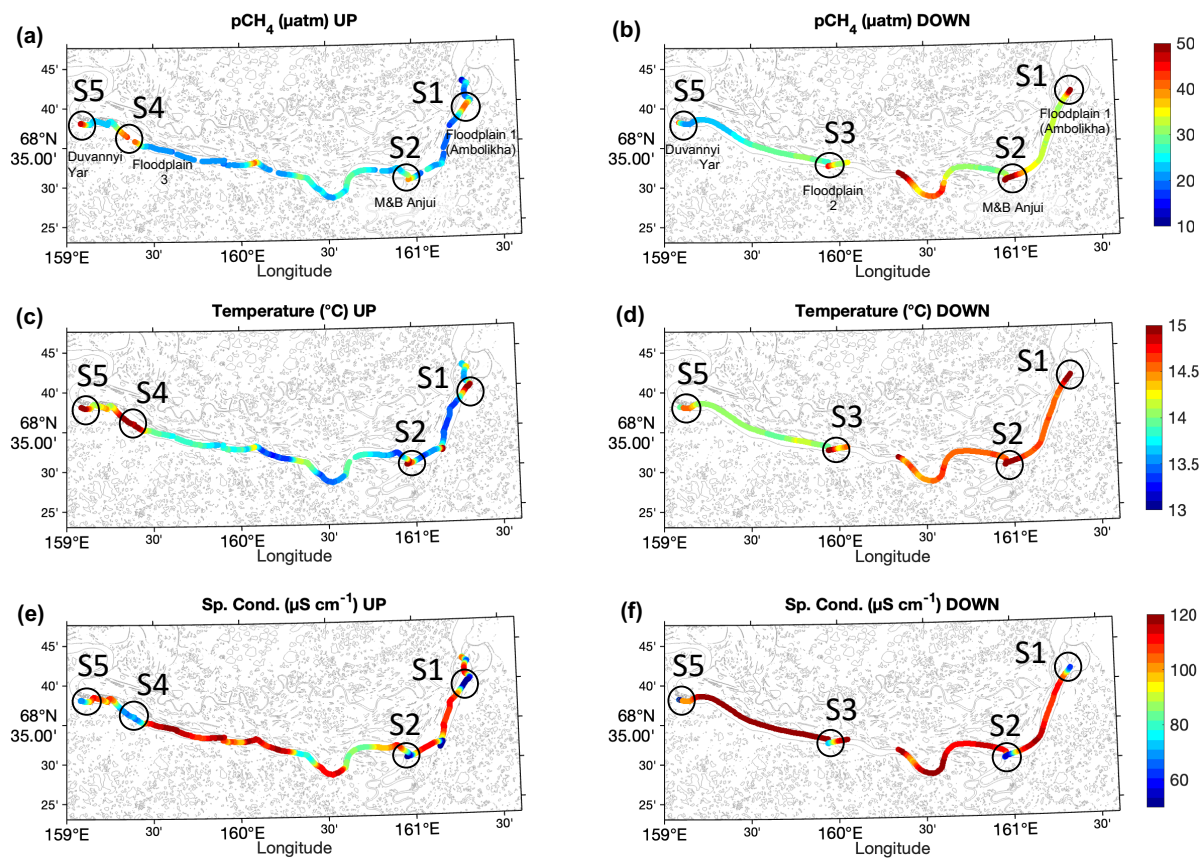


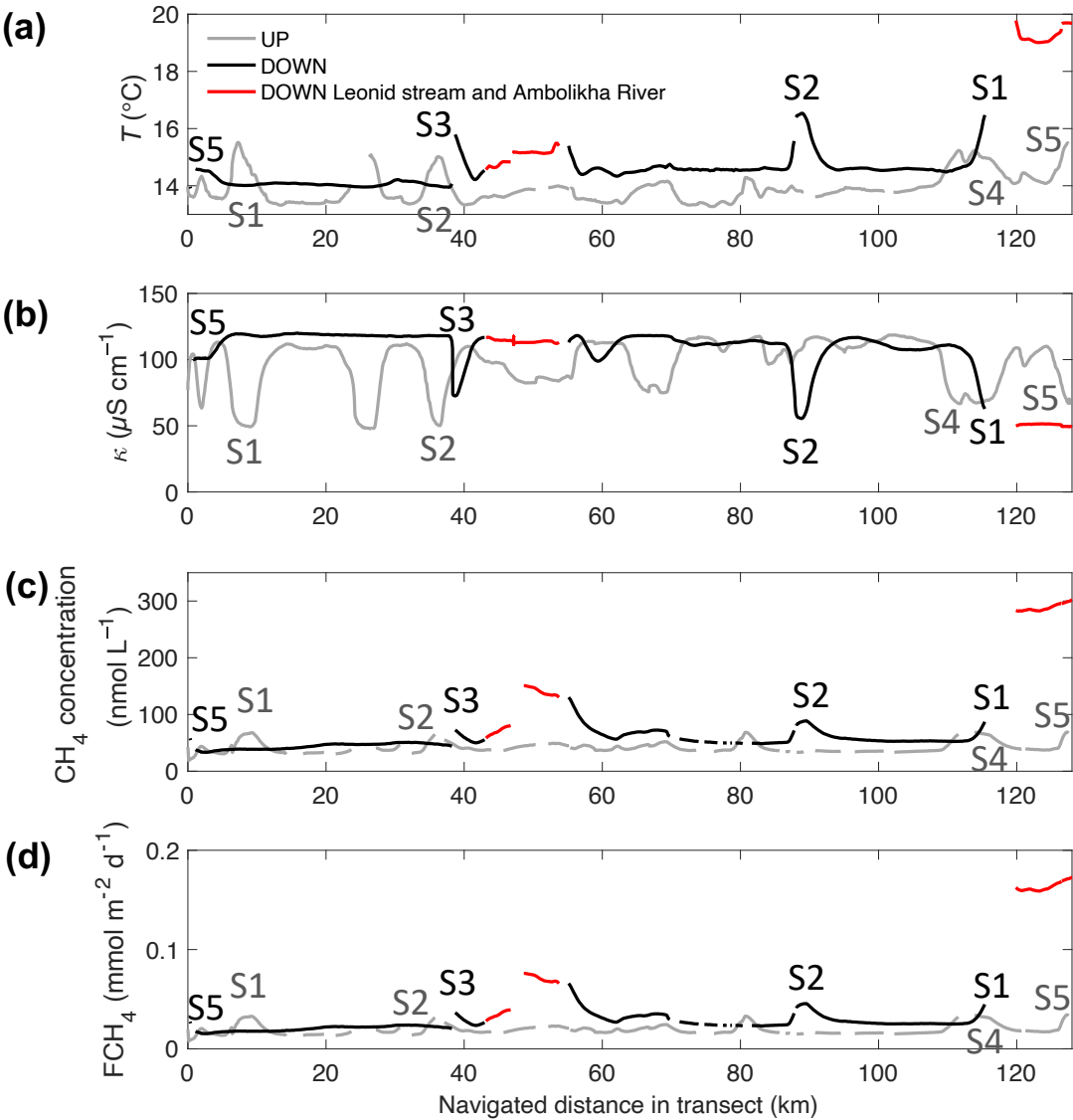
Fig. 2



1090

Fig. 3

Water properties measured along the UP and DOWN transect in Kolyma River (15-17 June 2019)

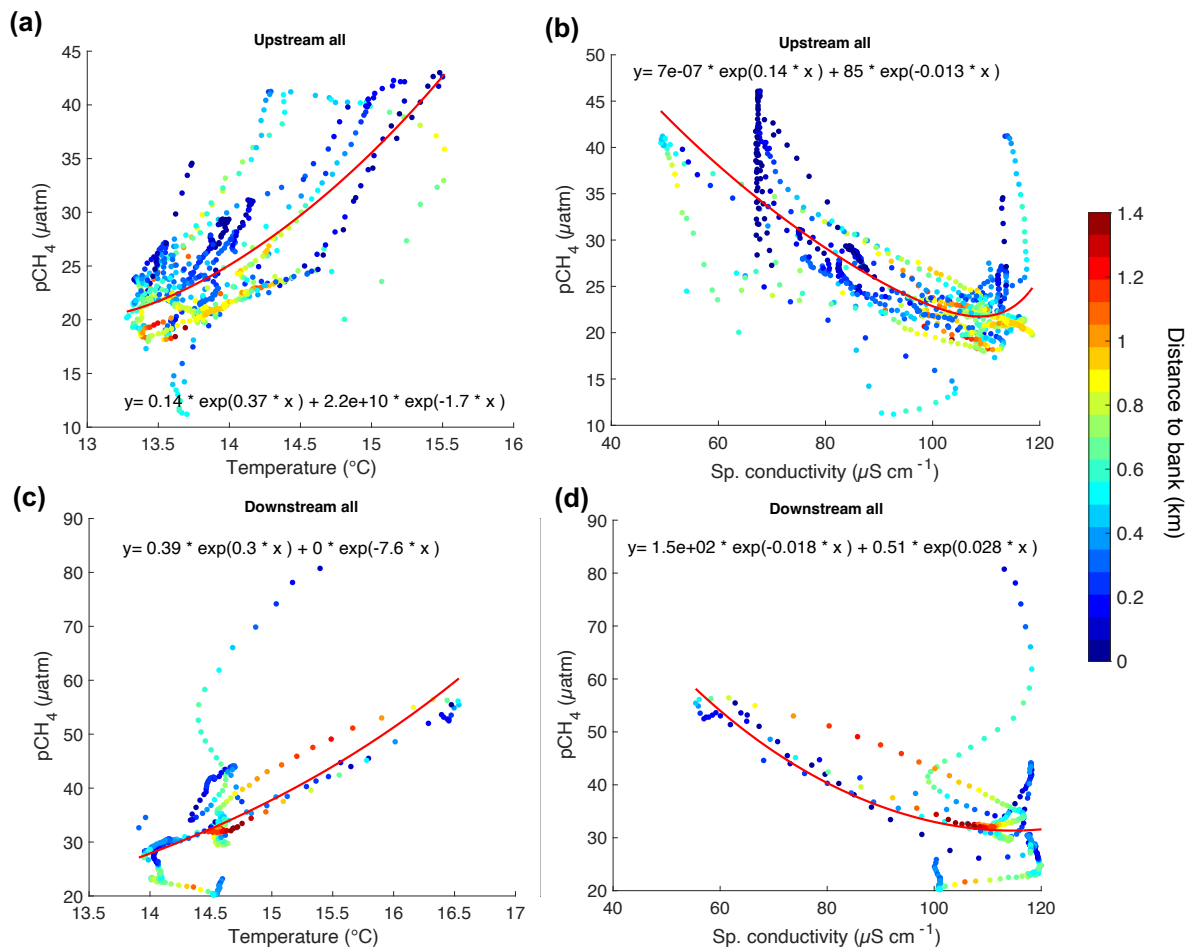


1095

1100

1105

Fig. 4



1110

1115

1120

1125

1130

Fig. 5

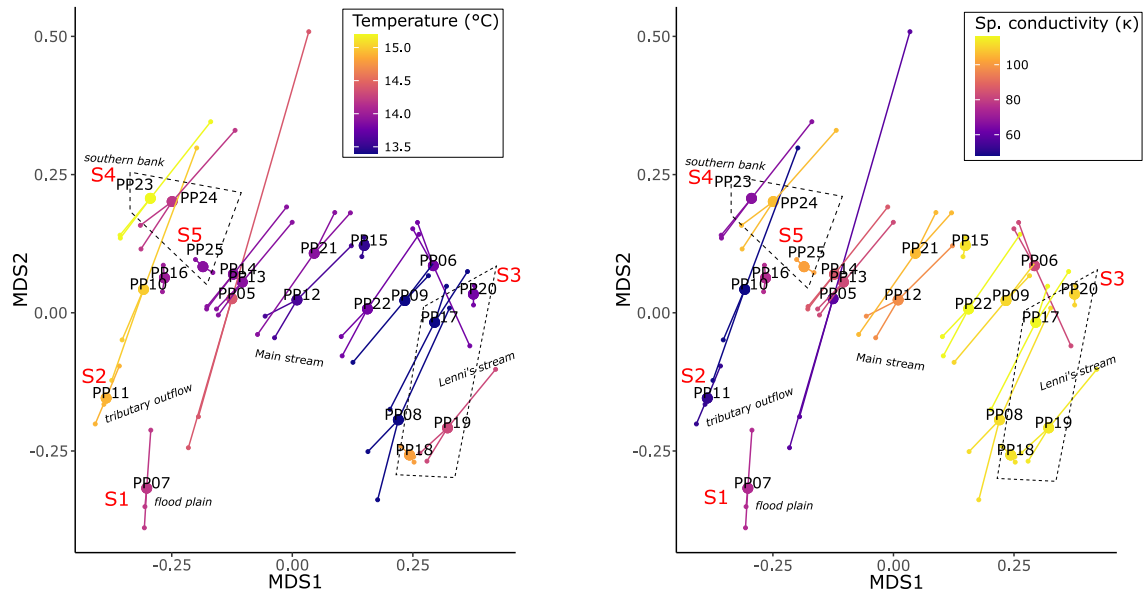
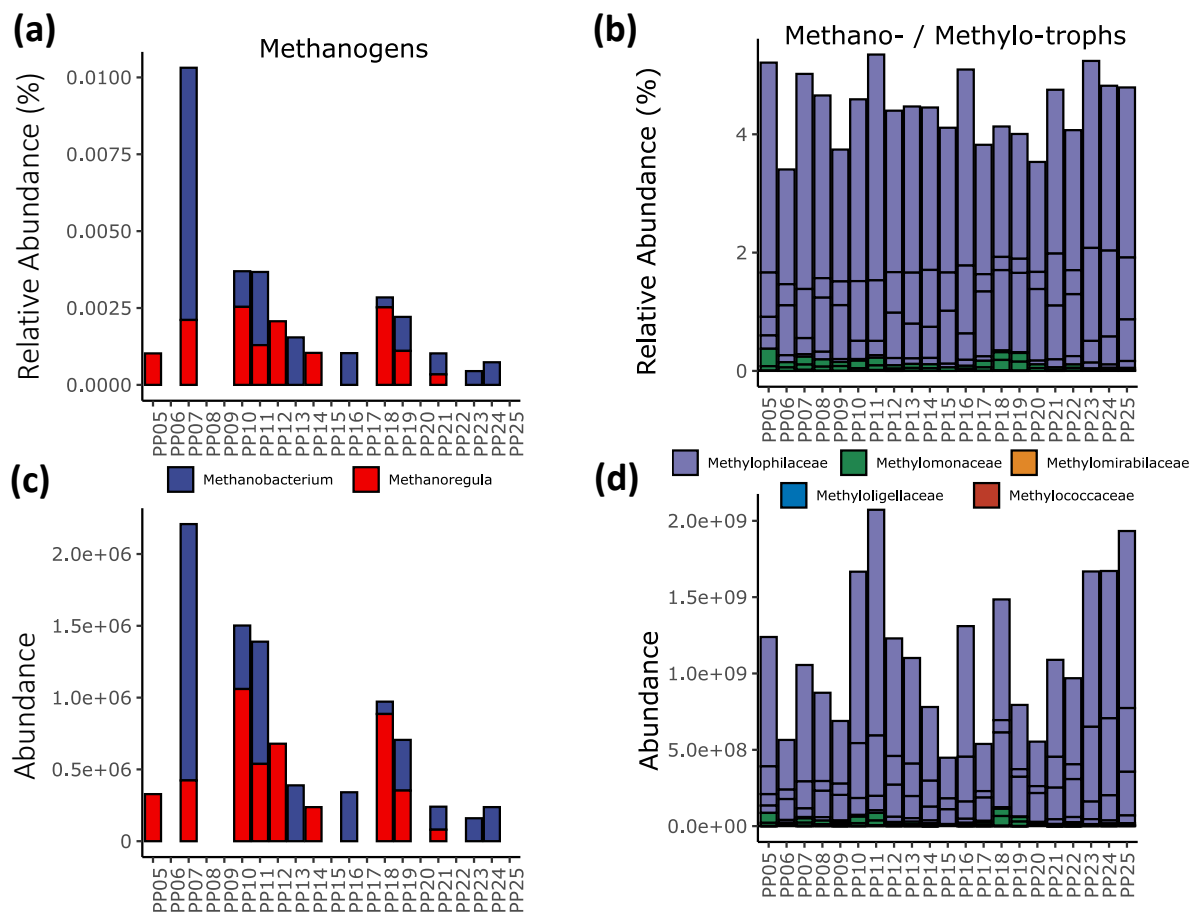
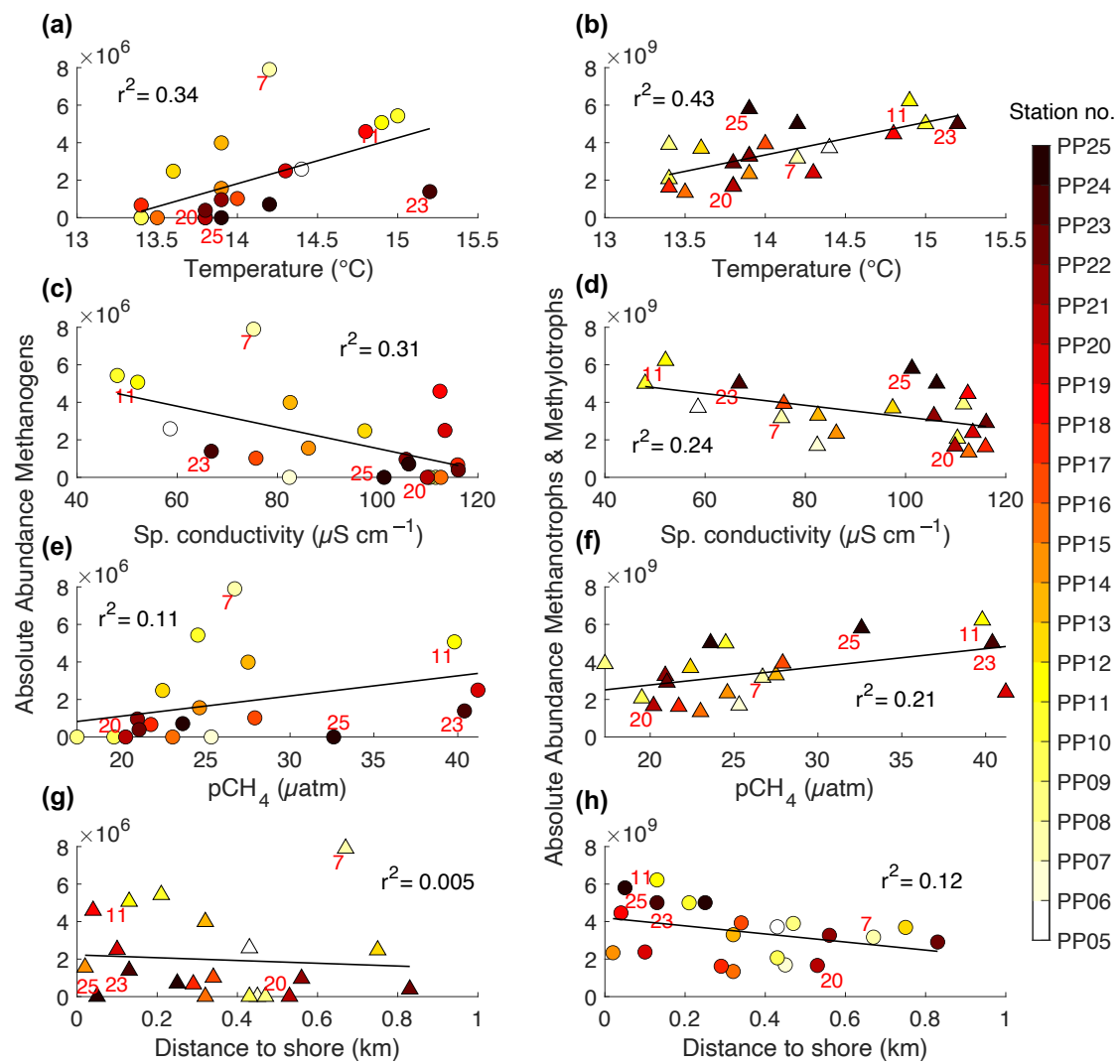


Fig. 6



1195

Fig. 7



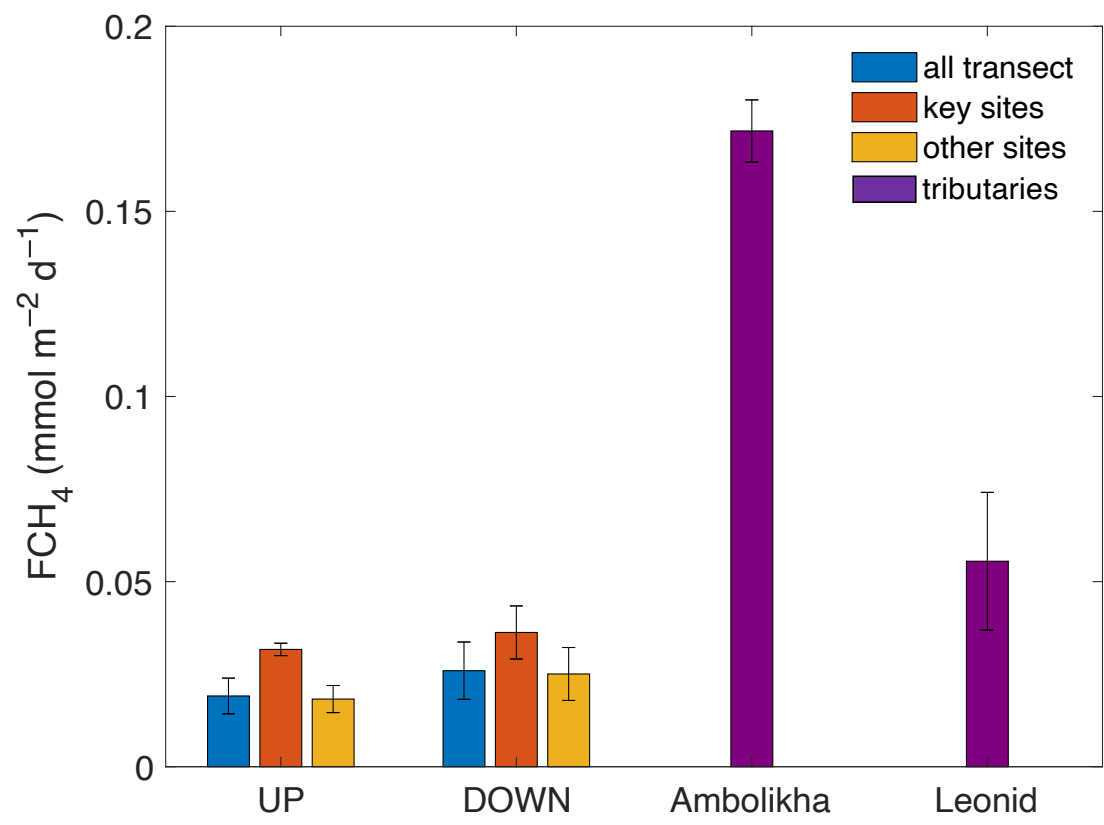
1200

1205

1210

1215

Fig. 8



1220

1225

Table 1 – Average \pm 1 std. deviation (minimum and maximum values below it) of $p\text{CH}_4$, the concentration of CH_4 (C_w), T and κ measured along the UP and DOWN transects in key sites (S1 – S5) and in the other sites of each transect. Measurements done in a tributary (Ambolikha River) and a stream (Leonid's stream) as part of the measurements during the DOWN transect are also shown.

Location	$p\text{CH}_4$ (μatm)	C_w (nmol L^{-1})	T ($^{\circ}\text{C}$)	κ ($\mu\text{S cm}^{-1}$)
Both transects	28.3 \pm 8.5 (11.2 – 80.7)	45.9 \pm 12.9 (18.9 – 130.2)	14.1 \pm 0.6	96.8 \pm 21.5
UP transect	25.8 \pm 6.7 (11.2 – 46.1)	41.5 \pm 9.2 (18.9 – 69.2)	13.9 \pm 0.6	92.2 \pm 22.2
UP key sites	39.4 \pm 4.3	65.0 \pm 3.0	14.9 \pm 0.3	65.1 \pm 6.9
UP other sites	23.8 \pm 4.3	39.9 \pm 7.0	13.9 \pm 0.5	95.8 \pm 20.9
DOWN transect	33.2 \pm 9.4 (20.2 – 80.7)	54.3 \pm 14.7 (33.3 – 130.2)	14.5 \pm 0.5	108.3 \pm 14.5
DOWN key sites	42.8 \pm 9.2	72.4 \pm 12.4	15.7 \pm 0.8	76.0 \pm 16.0
DOWN other sites	31.8 \pm 8.5	52.7 \pm 13.7	14.4 \pm 0.3	112.4 \pm 7.3
Ambolikha River (DOWN)	206.8 \pm 9.8 (191.7 – 222.9)	300.7 \pm 12.1 (282.2 – 320.7)	19.6 \pm 0.3	49.9 \pm 0.9
Leonid's stream (DOWN)	66.8 \pm 22.0 (37.0 – 92.9)	111.1 \pm 35.7 (60.8 – 150.7)	15.1 \pm 0.3	113.9 \pm 1.6

1230